Volume 6 • Number 3 • July 2012
ISSN: 1557-7244

Journal of APPLIED PACKAGING RESEARCH

Aim and Scope

The *Journal of Applied Packaging Research* is an international forum for the dissemination of research papers, review articles, tutorials and news about innovative or emerging technologies for the packaging industry. The journal is targeted towards the broad packaging community including packaging scientists and engineers in industry or academic research and development, food scientists and technologists, materials scientists, mechanical engineers, industrial and systems engineers, toxicologists, analytical chemists, environmental scientists, regulatory officers, and other professionals who are concerned with advances in the development and applications of packaging.

JOURNAL OF APPLIED PACKAGING RESEARCH—Published quarterly—January, April, July and October by DEStech Publications, Inc., 439 North Duke Street, Lancaster, PA 17602-4967.

This journal is recommended by The National Institute of Packaging Handling and Logistics Engineers (www.niphle.org).

Indexed by Chemical Abstracts Service.

Indexed and abstracted by Pira International.

Subscriptions: Annual $319 (Print), $319 (Electronic) and $344 (Print and Electronic). Single copy price $95.00. Foreign subscriptions add $45 per year for postage.

(ISSN 1557-7244)

DEStech Publications, Inc.
439 North Duke Street, Lancaster, PA 17602-4967, U.S.A.

CONTENTS

Research

Effect of Lateral Box Offset and Pallet Overhang on Compression Strength of Stacked Fiberboard Boxes and Impact on Stability

S. PAUL SINGH[1,*], JAY SINGH[2], KOUSHIK SAHA[3] and V. CHONHENCHOB[4]

[1]*Professor, College of Agriculture and Natural Resources, Michigan State University, East Lansing, MI*
[2]*Professor, Packaging Program, Cal Poly State University, San Luis Obispo, CA*
[3]*Assistant Professor, Packaging Program, Cal Poly State University, San Luis Obispo, CA*
[4]*Associate Professor, Packaging Program, Kasetsart University, Bangkok, Thailand*

ABSTRACT: The purpose of this study was to re-evaluate the effect of horizontal offset on the compression strength of stacked box configuration, and to evaluate the effect of pallet type, tie-sheet and stack configuration on compression strength of palletized loads. The last similar study was done in 1975. For this new study, presented in this paper, four different boxes of varying sizes and similar board combinations, made from single wall C-flute but different manufacturers were tested. The single box compression strength for each box size was determined to represent as the box control compression strength. The compression strength of control boxes were compared to overall strength of a three-high stack and in three different offset configurations. In addition, a set of perfectly aligned boxes stacked three high were compression tested for comparison with control and mis-aligned stacked boxes. The stack configurations were offset either in the length, width or diagonally (both length and width) with an offset distance of 12.7 mm, 25.4 mm or 38.1 mm (0.5, 1, and 1.5 inches). The second part of the study compared column stack configurations with a three high stack on a CHEP® (block style) or GMA (stringer style) wood pallets. The unitized loads also compared the effect of pallet overhang and role of tie-sheets in between layers.

*Author to whom correspondence should be addressed. E-mail: singh@msu.edu

1557-7244/12/03 129-20

1.0 INTRODUCTION

CORRUGATED BOXES are the most widely used form of transport packages providing containment and protection and being strong and economical. However exposure to various physical and climatic factors reduces strength during storage, shipping and handling. Boxes are stacked to provide utilization of space in storage facilities such as warehouses, while making the most optimum use of unimodal and inter-modal transport vehicles often referred to as "cube-utilization". Improper stacking and misalignment greatly reduces strength and can compromise the stability of a stacked load of boxes. This can cause damage to contents and pose safety concerns where exposure to human operators is present.

The compression strength of a corrugated fiberboard shipping container is affected by various factors including but not limited to dimensions, flute size, basis weight of liner/medium boards, exposure to temperature and humidity, creep, stacking configuration, as well as shipping and handling. Some of these climatic and physical factors can contribute towards the natural variation and degradation in the fiberboard and box compression strength or the box's ability to stack and support other filled and loaded boxes during storage and shipping. Both the corrugated and shipping industry has continuously studied the strength and the performance of a box, and its ability to survive the various elements of the distribution environment [1–3]. The most common method to evaluate the strength of an "empty" box and then predict it's degradation due to each individual factor is to perform a box compression test in the vertical orientation using a fixed rate compression tester. This information helps packaging engineers to predict performance for a given customer's transport and storage requirements.

The test methods [4,5] that have been accepted on a consensus basis globally to test empty box compression strength for more than forty years include:

- American Society of Testing and Materials (ASTM) test ASTM D642 "Standard Test Method for Determining Compressive Resistance of Shipping Containers, Components and Unit Loads", and
- International Standards Organization (ISO) equivalent ISO 12048 "Packaging-Complete, Filled Transport Packages-Compression and stacking test using a compression tester".

Shipping containers such as boxes are tested both with no contents

(empty), and filled with actual product. This information is used to compare their performance. The test method was originally developed by the paper industry through the Technical Association of Pulp and Paper Industries (TAPPI). TAPPI standard T804 [6], and was titled "Compression Testing of Fiberboard Containers". The authors caution readers of this paper that while this has been the most used and internationally accepted test method to measure strength of a fiberboard box, testing of filled containers will have a significantly different performance. Bulk liquids and bulk granular products when filled in a fiberboard box will cause it to bulge and most likely reduce strength of the box, whereas semi-rigid and rigid contents inside a fiberboard box will enhance overall package (combined box and contents) strength. However testing boxes containing hypothetical loads will not predict actual performance with "real" product or contents. It is for this reason the vast majority of tests performed to assess box compression strength are done on empty containers.

Box compression strength can be measured by using either a floating platen or a fixed platen on a compression testing machine (ASTM D642) [4]. A research study [7] showed that there was no significant difference in box compression strength between the two methods, comparing several types of boxes. The conclusions found that there is more variation associated with the compression strength performance between identical boxes as opposed to the difference between fixed and floating platen methods [7]. Additional studies have also shown that overall vertical compression strength of stacked boxes is lower than that of individually tested boxes [8]. Results show that in a three-high column stack of perfectly aligned boxes, strength reduction of 6–15% was observed in regular-slotted-container (RSC) style boxes, when compared to strength of a single box [8]. These effects are further magnified if the stack is misaligned [8, 9]. A study performed previously investigated the reduction in box compression strength where a stack was deliberately offset by fixed amounts of 12.7 mm, 25.4 mm or 38.1 mm (0.5, 1.0 and 1.5 inches) in the lateral and diagonally offset boxes [8]. The findings of this study show strength reductions of 59% in misaligned stacks as compared to individual box compression strength [8]. Since, shipping containers are stacked for storage and transportation on a pallet during transportation and warehousing, it is critical to minimize offsets to maintain stability.

Various previous studies have also been cited by Twede and Selke [10] that show the strength reduction effects to box compression

strength due to exposure to time (creep), temperature and humidity. The data presented is from earlier studies done by the Institute of Paper Chemistry. The text also cites factors for interlocking and column stacking of boxes on a pallet. The authors [10] state that column stacked aligned boxes on a pallet retain 85% of the box compression strength, whereas an interlock stack pattern that indicates an offset loading, will reduce strength of the stack by 50%.

During palletization and unitization of boxes on a pallet or slip-sheet, it is likely that misalignment among stacked layers may occur. Since, it has been established that vertical edges of a box contribute 2/3rd (66.7%) of the total box compression strength [1], significant strength reductions in stacked boxes will occur if they get misaligned during stacking [8]. A study was performed to compare loss of strength in stacked boxes due to increase in relative humidity and misalignment [11]. It was found that misaligned stacks with lateral or diagonal offset showed greater reduction in compression strength than changes due to humidity [11]. Results showed that stacked boxes lost 24% of strength due to exposure to high humidity of 90%, whereas misalignment in lateral and diagonally offset stacks showed a 52% reduction. It was noted that the combined effect of both high humidity and misalignment of "tested" boxes was 64%. This study found a significant important conclusion that combined effects of several factors (such as misalignment and humidity) do not show a cumulative effect based on the worse case of individual factors, as has been commonly taught in various packaging schools and institutes. Such large reductions using cumulative effect of combined factors, will cause packaging engineers to significantly overdesign fiberboard boxes resulting in both use of extra materials and increased cost. This is detrimental to today's increasing goals to reduce packaging and make sustainable choices.

It is also to understand the importance of interaction of several boxes on a layer stacked in a unitized configuration. This is typically how most boxes are loaded onto pallets or slip-sheets. Fiberboard boxes are typically stacked on a pallet and unitized using a stretch wrap film or banding for distribution and storage. Stack configurations, to make a unitized load of the shipping containers on a pallet, typically depend on individual size of boxes and pallet surface area, so as to fully optimize space utilization. The two commonly used stack configurations in the packaging industry are 'column' and 'interlocked'. Stacking operations in a packaging plant can be either automated or manual depending on the quantity of the production. Irrespective of the method of stacking,

a common issue that occurs is that the boxes in a layer may not completely cover the top layer of the pallet deck boards. Sometimes the bottom surfaces of boxes overhang off the pallet. The magnitude of this overhang may compromise the load bearing strength of the bottom layer, eventually causing pallet instability.

In 1975, Phil M. Ziegler, sent results of findings of a major research study conducted by the Container Corporation of America to all designers of corrugated packaging on behalf of the Technical Services of the Container Divisions. The report stated various factors that resulted in loss in top-to-bottom box compression strength due to pallet overhang, box misalignment and interlocking. It also stated that *"Without exception our customers underestimate the deterioration in top to bottom compression of containers when they are improperly handled and stacked in the distribution system"* [11]. The study further concluded that as much as 29% loss in compression strength is due to misalignment vertically and a 45% loss of compression is due to an interlocking pattern on a three high pallet unit. Data and test details on this extensive testing done on empty boxes was discussed by Ievans [8].

The results from this study were further presented in a Fibre Box Association document called *"CORRU~FACTS"* that summarized "corrugated facts for users of corrugated packaging" [4]. This document summarized the results of the study as:

1. Pallet Overhang can reduce top to bottom compression up to 32%.
2. Wooden pallets can reduce top to bottom compression up to 32%.
3. Interlocked patterns can reduce top to bottom compression up to 55%.

In addition, this document stated that to provide load stability of stacked corrugated boxes in transit a shipper had four options. These were reported as:

1. Use of anti-skid treatment on the flaps of the containers to increase the coefficient of friction.
2. Spot-gluing the tiers of a pallet load
3. Use of a plastic or corrugated shroud.
4. Use of a Master Pack

It also concluded that "whenever possible make sure that you utilize *'vertical (columnar) stacking rather than interlocked stacking'*".

The results of this previous study were further investigated and published in 1979. This study investigated the effect of various amounts of overhang and pallet stack configurations and found that the percent loss in strength for a palletized box configuration varied considerably depending on the box geometry, board grade and flute size [1]. The results showed that the percent loss in palletized box compression strength as a function of overhang could range between 23–49% depending on the amount and type of overhang (along length, width or both sides) [1]. A more recent research study was conducted where three palletized loads of two-piece plastic cans were stacked in various staggered positions to evaluate the effect of off-set on stack stability [9]. It was discovered that a 153 mm (6 in) pallet offset in the middle pallet and a 204 mm (8 in) pallet offset on the top pallet made the three high palletized loads unstable resulting in a tip-over of the top two stacked pallet loads [9]. This can have serious outcomes both in product loss as well as human safety in warehouse aisles where operators function.

Therefore, the focus of this study was to evaluate the effect of pallet type, tie-sheet and stack configuration on compression strength of a palletized load of boxes with different dimensions, and reassess the changes in expected loss of strength due to factors such as misaligned boxes, types of pallets and pallet overhang.

As stated in the introduction section of this paper, no comprehensive study has ever been conducted on paper corrugated boxes to evaluate performance similar to the 1975 project over the past 30 years. It is well known that the North American paper manufacturing industry has been able to make thinner and stronger paper over the last three decades. This has been achieved by increasing recycling content using better re-pulping processes, and calendering, thereby making it thinner yet stronger due to more fiber.

This paper is one of three papers that discuss the results of two independent studies done with single wall C-flute corrugated boxes. The first study has been published in two papers, one discussing the loss of strength to individual boxes due to stacking and offset [12], and the second paper [13] published the results of pallets, tie sheets, pallet patterns. This first study discussed in the above described papers, compared four different size boxes obtained from three different manufacturers, and used different data and boxes than what is presented in this study and paper.

Four different sized boxes were each obtained from three different manufacturers for a total of four different sized boxes (Table 1).

Table 1. Sample Box Specifications.

Box Type	ECT Kgf/cm	Length (m)	Width (m)	Height (m)	Fiberboard Box Supplier
Box 1	5.71	0.48	0.38	0.25	Coastal Container, MI
Box 2	5.71	0.48	0.33	0.15	Coastal Container, MI
Box 3	5.71	0.38	0.25	0.25	South Haven Packaging, MI
Box 4	5.71	0.41	0.30	0.25	Michcor Container, MI

2.0 MATERIALS AND METHODS

Four regular slotted fiber board boxes of varying dimensions made from same board grade and of C-flute with an ECT of 5.71 Kgf/cm were selected for this study (Table 1). The test samples were obtained from three different box suppliers located in Michigan, United States. These boxes were erected, glued, and pre-conditioned at 23°C (73°F) and 50% RH in accordance with "standard" conditions described in ASTM D4332 [12], for at least 72 hours prior to compression testing in accordance with ASTM D642 [4] (Figure 1). In the first phase of the study 30 samples of each box type were tested for individual box com-

Figure 1. *Boxes pre-conditioned at standard conditions for at least 72 hours.*

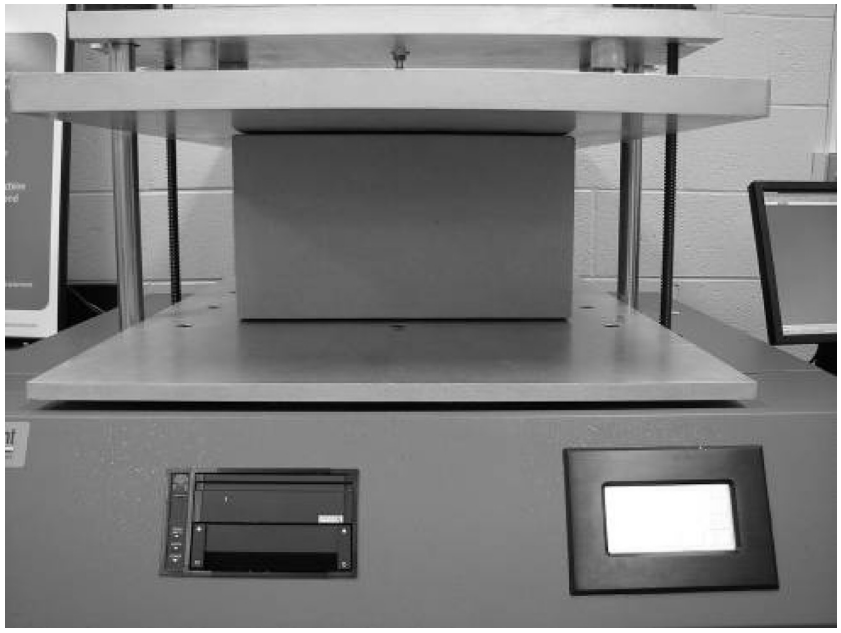

Figure 2. *Test set up for single box compression strength.*

pression strength using a compression tester (Lansmont Corporation, Monterey, CA). The vertical compression strength of individual boxes for each type as seen in Table 1 was treated as "control" (Figure 2). Data measured with the three-high stacking and misalignment (offset) was compared to these "control" compression strength values (Table 3).

The second phase of this study compared the box compression strength of the three-high stack, with three different amounts of offsets (Length, Width and Diagonal or both sides) as shown in Figures 3–5. The offset amounts used were 12.7, 25.4 and 38.1 mm (0.5, 1.0 and 1.5 inches). A "length" offset means that the bottom box and the top box are offset by an amount of 0.5, 1.0 or 1.5 inches only with respect the

Table 2. Single Box Compression Strengh.

Box Type	Compression Strength (Kg)	Max	Min
Box 1	227.7 ± 14.7	261.9	196.5
Box 2	280.8 ± 20.8	317.0	230.6
Box 3	138.1 ± 15.1	160.4	102.4
Box 4	191.2 ± 16.2	233.4	164.7

Table 3. Experimental Design for Different Test Treatments.

	Number of Replicates			
Stack Offset	12.7 mm	25.4 mm	38.1 mm	Perfectly Aligned
Length Panel	10	10	10	
Width Panel	10	10	10	10
Two Adjacent Panel	10	10	10	

length orientation. They are perfectly aligned in the width dimension. Similar is the definition of "width" offset. However a "diagonal" offset means that the offset between the bottom and top boxes is in both the length and width dimension.

A set of perfectly aligned boxes stacked three-high were compression tested for comparison with "control" and a misaligned stack. Ten replicates of compression testing were performed for each test set up, and the experimental design is shown in Table 3. All tests were performed under "standard" conditions.

The third phase of this study compared the effects of unitization and interaction with different types of wood pallets. Two types of standard wooden pallets measuring 1219 × 1016 × 127 mm (48 × 40 × 5 in) were used. The first type of pallet was in conformance to the requirements of the Grocery Manufacturers Association (GMA) (Figure 6). The second type of pallet was manufactured per the specifications of the Commonwealth Handling Equipment Pool organization (CHEP®) (Figure 4). CHEP® is the world's largest container and pallet leasing company and issues, collects, repairs and reissues about 300 million pallets and containers to assist manufacturers, distributors and retailers to transport their products safely and efficiently [13]. GMA pallets are amongst the most commonly used pallet styles in North America and account for 30% of all new wood pallets produced in the United States [13]. ISO also recognizes the GMA pallet footprint as one of its

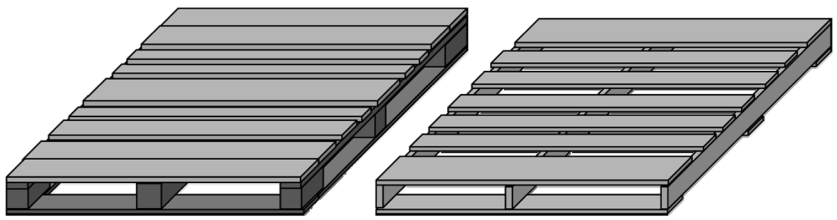

Figure 3. *Pallet Types used in Study.*

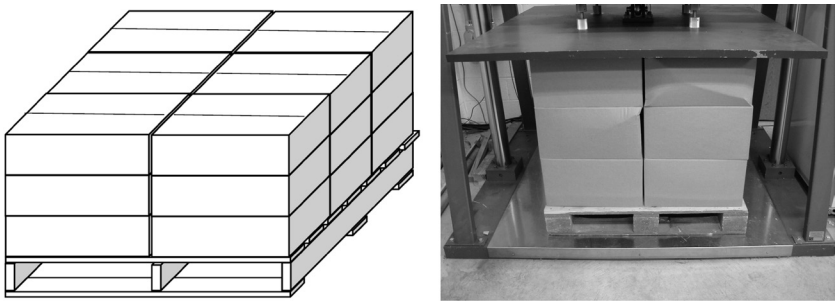

Figure 4. *Palletized Box Stack Configuration for Control—Column Pattern.*

six standard sizes. The major application of these pallets is for grocery distribution in North America. The CHEP® pallet has a larger top deck surface coverage than the GMA pallet.

This phase of the study was designed to determine the effect of pallet type, tie-sheet and stack configuration on the compression strength of a unitized load. The four different stack configurations considered for this study were column stack as "control", inter-lock, overhang and inter-lock-overhang stacks as shown in Figures 7–10. The unitized load compression strength was performed on all four stack configurations with a tie-sheet between each layer and repeated without a tie-sheet between the layers. Three replicates were performed for each test set up. The experimental design for this study is shown in Table 4. The column stack pallet configuration which represented the control was compared with the three stack configurations with either a tie-sheet in between layers or no tie-sheet between layers of stacked boxes. Compression testing was done in accordance with ASTM D642 using a compression tester (Lansmont, Monterey, CA) under "standard" conditions. This configuration was similar to that done in the previous research by Ziegler [11], and the same configuration was requested by the Consortium of Dis-

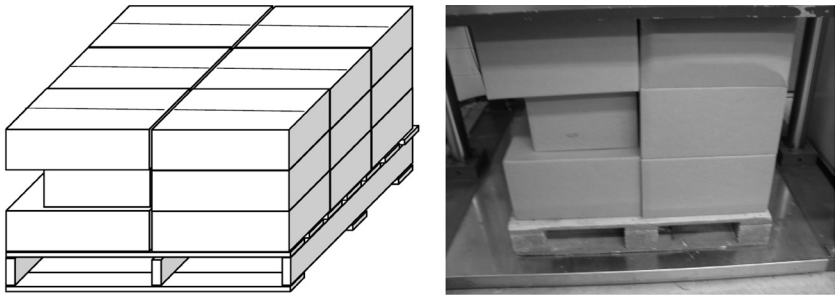

Figure 5. *Palletized Box Stack Configuration for Interlocked Pattern.*

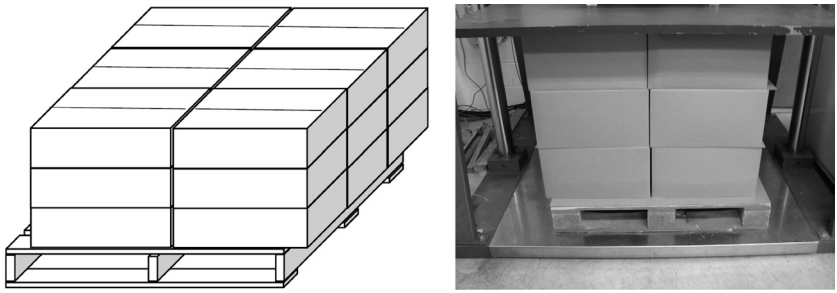

Figure 6. *Palletized Box Stack Configuration for Interlocked Pattern.*

tribution Packaging Research members as part of this project. The box sizes were selected by the research group and provided directly from the manufacturer to the distribution packaging test labs at Michigan State University and Cal Poly State University.

3.0 RESULTS AND DISCUSSION

The data representing the average single box compression strength and that of a perfectly aligned three-high stack of boxes is shown in Tables 2 and 5. The loss of strength in corrugated boxes as a function of

Table 4. Experimental Design for Different Test Treatments.

Type of Box	Pallet Type		Stack Configuration				
Box 1	CHEP®	Tie-sheet	Control	Interlocked	Overhang	Interlocked	Overhang
Box 1	CHEP®	No Tie-sheet	Control	Interlocked	Overhang	Interlocked	Overhang
Box 1	GMA	Tie-sheet	Control	Interlocked	Overhang	Interlocked	Overhang
Box 1	GMA	No Tie-sheet	Control	Interlocked	Overhang	Interlocked	Overhang
Box 2	CHEP®	Tie-sheet	Control	Interlocked	Overhang	Interlocked	Overhang
Box 2	CHEP®	No Tie-sheet	Control	Interlocked	Overhang	Interlocked	Overhang
Box 2	GMA	Tie-sheet	Control	Interlocked	Overhang	Interlocked	Overhang
Box 2	GMA	No Tie-sheet	Control	Interlocked	Overhang	Interlocked	Overhang
Box 3	CHEP®	Tie-sheet	Control	Interlocked	Overhang	Interlocked	Overhang
Box 3	CHEP®	No Tie-sheet	Control	Interlocked	Overhang	Interlocked	Overhang
Box 3	GMA	Tie-sheet	Control	Interlocked	Overhang	Interlocked	Overhang
Box 3	GMA	No Tie-sheet	Control	Interlocked	Overhang	Interlocked	Overhang
Box 4	CHEP®	Tie-sheet	Control	Interlocked	Overhang	Interlocked	Overhang
Box 4	CHEP®	No Tie-sheet	Control	Interlocked	Overhang	Interlocked	Overhang
Box 4	GMA	Tie-sheet	Control	Interlocked	Overhang	Interlocked	Overhang
Box 4	GMA	No Tie-sheet	Control	Interlocked	Overhang	Interlocked	Overhang

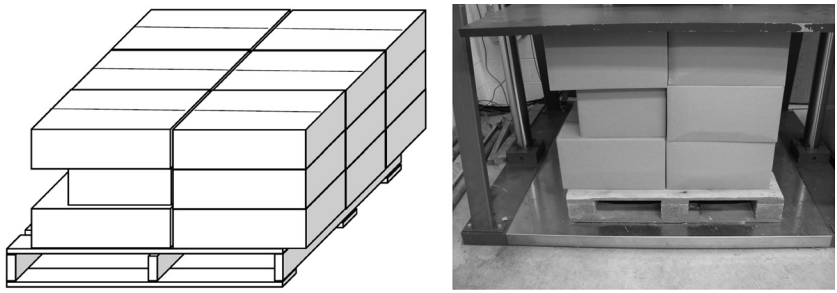

Figure 7. *Palletized Box Stack Configuration for Interlocked Overhang Pattern.*

lateral and diagonal offset as shown in Figures 3–5 was also conducted. The average compression strength of three-high stack of boxes with the three different levels of misalignment offset as shown in Table 6 was also measured.

The single box measured compression strength was the highest for Box 2 followed by Box 1, Box 4 and Box 3 (Table 2). Data analysis showed that the standard deviation in compression strength of identical boxes ranged between 6 to 8% for all types of boxes. A similar trend was observed for the box compression strength for perfectly aligned stack of boxes, where Box 2 was recorded to have the highest box compression strength followed by Box 1, Box 4 and Box 3. However, the standard deviation in compression strength of identically stacked boxes with no misalignment was between 4 to 10% for all types of boxes (Table 5). This shows that the natural variation in single box compression

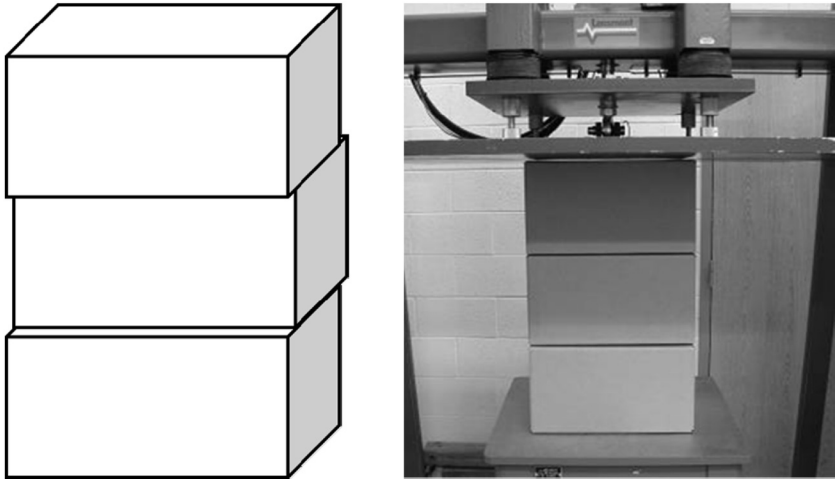

Figure 8. *Test setup for misaligned three-high stacks of boxes along the long edge.*

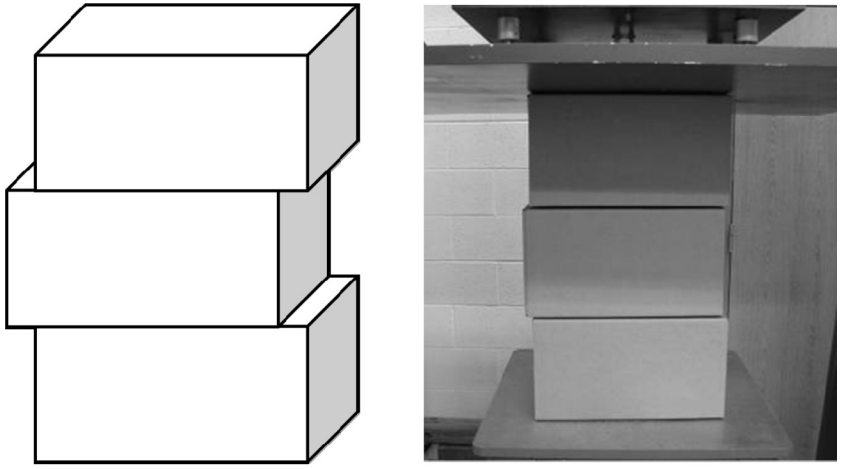

Figure 9. *Test setup for misaligned three-high stacks of boxes along the wide edge.*

strength further contributes to further variation in a stack of perfectly aligned boxes. Data for this is shown Tables 2 and 5. The percent loss in compression strength of a perfectly aligned stack of boxes as compared to the "control" box compression strength of an un-stacked box ranged from 6.5% to 19% (Table 7). This finding agrees with a study done earlier, where the percent reduction of compression strength of three-high stacked boxes as compared to and un-stacked box ranged from 6–15% [3]. These results are based on the data from the various tests conducted and the percent reduction is based on a percent ratio of the difference

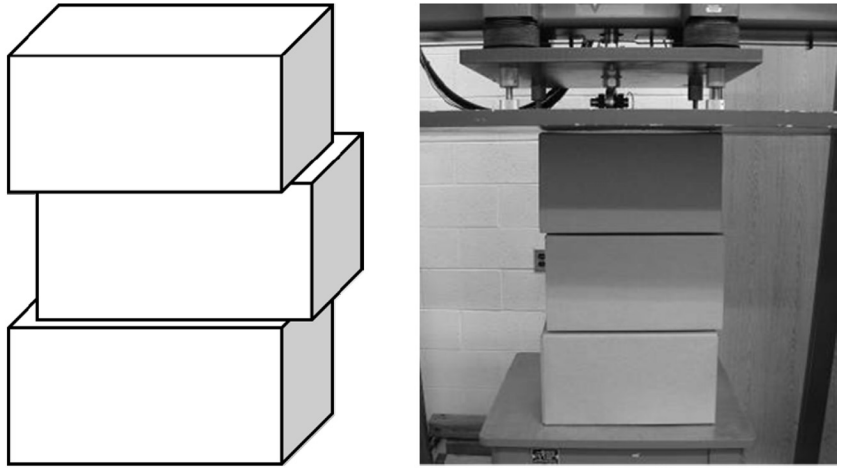

Figure 10. *Test setup for misaligned three-high stacks of boxes along the adjacent edges.*

Table 5. Box Compression Strength of Aligned Stack.

Box Type	Compression Strength (Kg) Control
Box 1	212.9 ± 16.2
Box 2	227.5 ± 11.5
Box 3	127.0 ± 16.5
Box 4	176.4 ± 19.4

between strength of control boxes and stacked boxes to the strength of control boxes.

In general, stacked boxes result in lower overall compression strength (CS), typically representing the CS of the weakest box in the stack, as compared to an individual box tested for compression strength. However if all stacked boxes have individual strength higher than an individual box and if a perfectly aligned stack is attained this is not true.

Similar trends were observed when comparing box compression strength of single boxes to the various misaligned stacks of boxes (Table 6). The percent loss in compression strength was observed to be the highest for misaligned stacks with an offset distance of 38.1 mm (1.5 in) followed by the 25.4 mm (1.0 in) and 12.7 mm (0.5 in) offset

Table 6. Box Compression Strength of Mis-aligned Stack.

	Compression Strength (Kg)		
	Length Panel		
Box Type	Offset 12.7 mm	Offset 25.4 mm	Offset 38.1 mm
Box 1	202.6 ± 8.3	154.7 ± 19.1	137.7 ± 35.6
Box 2	196.6 ± 11.8	168.6 ± 24.2	149.5 ± 12.1
Box 3	94.4 ± 4.7	84.3 ± 8.3	80.6 ± 6.5
Box 4	145.3 ± 8.6	113.7 ± 16.3	103.0 ± 9.7
	Width Panel		
Box 1	185.7 ± 10.9	169.6 ± 10.1	164.3 ± 9.7
Box 2	206.7 ± 16.1	193.0 ± 24.2	171.0 ± 13.8
Box 3	91.9 ± 11.1	80.6 ± 8.2	76.1 ± 6.5
Box 4	149.6 ± 14.4	130.7 ± 7.1	115.9 ± 14.2
	Adjacent Panels		
Box 1	186.2 ± 9.2	147.2 ± 5.2	109.1 ± 8.3
Box 2	188.2 ± 8.9	152.8 ± 5.3	113.3 ± 10.8
Box 3	95.7 ± 6.1	76.7 ± 5.4	54.5 ± 0.6
Box 4	136.8 ± 17.0	105.0 ± 13.2	89.1 ± 19.9

Table 7. Percent Loss in Box Compression Strength of Aligned Stack.

Box Type	Percent Loss Compression Strength
Box 1	*6.5%
Box 2	19.0%
Box 3	8.0%
Box 4	7.8%

*Percent loss in compression strength shown in Table 5 compared to individual box compression strength shown in Table 1.

in the lateral directions along the length and the width (Table 8) for all four box types. However, the effect of offset direction on box compression strength was the highest when a stack of box was diagonally offset by 38.1 mm (1.5 inches). Table 6 shows the data for boxes stacked with different offset or misalignment conditions. It is clear that even the smallest offset of 12.7 mm or 0.5 inch produces a large reduction in compression strength. Additional offset amounts continued to show additional reduction in strength.

Table 8. Percent Loss in Box Compression Strength of Mis-aligned Stack of Corrugated Box.

	Compression Strength (Kg)		
	Length Panel		
Box Type	**Offset 12.7 mm**	**Offset 25.4 mm**	**Offset 38.1 mm**
Box 1	*11%	32%	40%
Box 2	30%	40%	47%
Box 3	32%	39%	42%
Box 4	24%	41%	46%
	Width Panel		
Box 1	18%	26%	28%
Box 2	26%	31%	39%
Box 3	33%	42%	45%
Box 4	22%	32%	39%
	Adjacent Panels		
Box 1	18%	35%	52%
Box 2	33%	46%	60%
Box 3	31%	44%	61%
Box 4	28%	45%	53%

*Percent loss in compression strength shown in Table 6 compared to individual box compression strength shown in Table 1.

Table 9. Palletized Box Compression Strength on CHEP® with Tie-Sheet.

	Control (Kg)	Interlocked (Kg)	Overhang (Kg)	Interlocked Overhang (Kg)
Box 1	1124	933 ± 60.7	1097 ± 29.0	858 ± 3.2
Box 2	1195	1028 ± 38.3	1258 ± 79.9	997 ± 86.6
Box 3	613	588 ± 10.4	574 ± 43.0	498 ± 13.4
Box 4	963	661 ± 100.3	934 ± 58.1	753 ± 7.4

The data for the column stack configuration (control) of unitized boxes was found to have the highest compression strength compared to the three-stack configurations on CHEP® or GMA pallets, with or without a tie-sheet between layers for all box dimensions. Column stack configuration of palletized boxes with tie-sheets was also found to be higher than ones with no tie-sheets (Tables 9–12). The tie-sheets transfer the load over the entire layer of lower boxes thereby acting as a load-spreader and discounting the effect of the weakest box in the stack.

The interlocked palletized stack configuration showed lower total compression strength than the column stack configuration (Tables 9–12). This trend was observed on both types of pallets studied with or without ties sheet between layers. This shows that an interlocked stacking pattern has a larger effect on reducing overall unitized load compression strength than a column stack with a 25.4 mm overhang as shown in Figure 9. An interlocked pattern provides a more stable configuration in handling, however as the boxes are not aligned along all the box edges and corners for each layer, this configuration results in a lower compressive resistance compared to a column stack configuration.

Overall the CHEP® pallets provided a higher palletized box compression strength than palletized boxes placed on a GMA pallet. The spacing between the top deck-boards on a CHEP® pallet is much closer as compared to standard GMA pallets. Therefore the bottom layer (load

Table 10. Palletized Box Compression Strength CHEP® with no Tie-Sheet.

	Control (Kg)	Interlocked (Kg)	Overhang (Kg)	Interlocked Overhang (Kg)
Box 1	1050	773 ± 37.1	1126 ± 53.1	764 ± 9.5
Box 2	1100	827 ± 24.1	1204 ± 121.9	890 ± 17.0
Box 3	461	345 ± 111.4	387 ± 36.6	345 ± 15.8
Box 4	1002	796 ± 90.3	949 ± 44.0	811 ± 23.6

Table 11. Palletized Box Compression Strength on GMA with Tie-sheet.

	Control (Kg)	Interlocked (Kg)	Overhang (Kg)	Interlocked Overhang (Kg)
Box 1	1228.8	897.2 ± 89.3	1067.1 ± 93.9	820.2 ± 77.5
Box 2	1367.1	938.1 ± 26.2	1030.4 ± 79.7	859.5 ± 39.8
Box 3	584.2	492.6 ± 21.6	582.8 ± 32.1	520.2 ± 10.6
Box 4	927.1	801.1 ± 19.1	915.5 ± 107.7	754.1 ± 14.7

Table 12. Palletized Box Compression Strength on GMA with No Tie-Sheet.

	Control (Kg)	Interlocked (Kg)	Overhang (Kg)	Interlocked Overhang (Kg)
Box 1	1055	762 ± 77.3	854 ± 31.5	692 ± 55.6
Box 2	932	714 ± 143.4	877 ± 61.4	704 ± 34.8
Box 3	549	467 ± 5.9	496 ± 39.2	396 ± 37.9
Box 4	965	623 ± 80.2	803 ± 68.7	636 ± 101.3

Table 13. Percent Loss of Palletized Box Compression Strength on CHEP® with Tie-Sheet.

	Interlocked (Kg)	Overhang (Kg)	Interlocked Overhang (Kg)
Box 1	17%	2%	24%
Box 2	14%	–	17%
Box 3	4%	6%	19%
Box 4	31%	3%	22%

Table 14. Percent Loss of Palletized Box Compression Strength on CHEP® with no Tie-Sheet.

	Interlocked (Kg)	Overhang (Kg)	Interlocked Overhang (Kg)
Box 1	26%	–	27%
Box 2	25%	–	19%
Box 3	25%	16%	25%
Box 4	21%	5%	19%

Table 15. Percent Loss of Palletized Box Compression Strength on GMA with Tie-Sheet.

	Interlocked (Kg)	Overhang (Kg)	Interlocked Overhang (Kg)
Box 1	27%	13%	33%
Box 2	31%	25%	37%
Box 3	14%	1%	19%
Box 4	14%	1%	19%

bearing layer) without tie-sheet on a CHEP® pallet is not damaged as boxes on GMA pallet.

The palletized box compression strength of boxes between respective stack configurations on CHEP® and GMA pallets with or without tie-sheets between layers was also compared. It was observed that use of tie-sheets between layers had a positive effect on the palletized box compression strength. The data in Tables 9 and 11 indicate that the load bearing layer is able to sustain higher compressive strength when a tie-sheet is placed on the pallet deck for both CHEP® and GMA pallets. Overall tie sheets provide a positive effect (higher total compression resistance) for both GMA and CHEP® pallets.

The percent loss in box compression strength in a palletized configuration using CHEP® pallets with and without slip sheets is shown in Tables 13 and 14, and similar data for GMA pallets is presented in Tables 15 and 16.

4.0 CONCLUSIONS

The following conclusions were reached in this study:

1. A perfectly aligned stack of boxes shows a 6–19% reduction in

Table 16. Percent Loss of Palletized Box Compression Strength on GMA with no Tie-Sheet.

	Interlocked (Kg)	Overhang (Kg)	Interlocked Overhang (Kg)
Box 1	28%	19%	34%
Box 2	23%	6%	24%
Box 3	15%	10%	28%
Box 4	35%	17%	34%

compression strength when compared to the individual compression strength of a box. Stack misalignment contributes to significant reduction in box compression strength as shown in the results.

2. Reduction in box compression strength was the highest for stack offset along both the adjacent panels followed by length and width panel.
3. The compression strength of unitized and stacked boxes in an inter-lock pattern is lower than that of column stacked boxes, and is dependent on the size and shape of the box.
4. The compression strength of palletized empty corrugated boxes on a CHEP® pallet is higher than compression strength of similar stacked boxes on a GMA specified wood pallet.
5. The loss in compression strength with no tie-sheet between layers is more than with a tie-sheet when comparing stacked empty and palletized boxes.
6. The average loss in compression strength due to three-high palletization is 25% or boxes retain 75% of their original empty box compression strength.
7. The average loss in compression strength due to over-hang on a three high stacked boxes on a pallet is 13% or boxes retain 87% of their original empty box compression strength.
8. Loss of strength in stacked configurations affects the overall stability of stacked loads during warehousing and storage and can result in fatal results in the form of damage or injury.

REFERENCES

1. Fiber Box Association, Corru~Facts, Corrugated Facts for Users of Corrugated Packaging, February 1979, Fibre Box Association, Chicago, IL, USA.
2. Patel, P., Nordstrand, T. and Carlssonb, L. A., Local buckling and collapse of corrugated board under biaxial stress, *Composite Structures,* 1997, 39(1-2):93–110.
3. Biancolini, M. E. and Brutti, C., Numerical and Experimental Investigation of the Strength of Corrugated Board Packages, *Packag.Technol. Sci.,* 2003, 16:47–60.
4. ASTM D642, Standard Test Method for Determining Compressive Resistance of Shipping Containers, Components and Unit Loads. *2010 Annual Book of American Society of Testing and Materials,* Vol. 15.10, ASTM, West Conshohocken, PA, USA.
5. ISO 12048 Packaging—Complete, filled transport packages—Compression and stacking tests using a compression tester, 1995. International Organization for Standardization, Geneva, Switzerland.
6. T 804 om-06, Compression Test of Fiberboard Shipping Containers, 2006-2007 TAPPI Test Methods, Technical Association of the Pulp and Paper Industry, South Norcross, GA 30092.
7. Singh, S. P., Burgess, G. and Langlois, M., Compression of single-wall corrugated containers using fixed and floating test platens, *J. Testing and Evaluation,* 1992 20(4):318–320.

8. Ievans, U. I., The effect of warehouse mishandling and stacking patterns on the compression strength of corrugated boxes, *TAPPI,* Vol. 58, No. 8, August, 1975
9. Singh, S. P. 'Instability of stacked pallet loads due to misalignment' *J. Testing and Evaluation,* 1999 27(5):349–353.
10. Twede, D. and S. Selke, *Cartons, Crates, Corrugated Board: Handbook of Paper and Wood Packaging Technology,* ISBN No. 1-932078-42-8, DEStech Publications, Inc., Lancaster, PA, USA.
11. Kellicutt, K. Q. Effect of contents and load bearing surface on compressive strength and stacking life of corrugated containers. *TAPPI,* 1963, 46(1): 151A.
12. ASTM Standard D 4332-01 (2006) "Standard Practice for Conditioning Containers, Packages, or Packaging Components for Testing". ASTM International. ASTM International, West Conshohocken, PA, 2007, DOI: 10.1520/D4332-01R06.
13. Clarke, J., "Pallets 101: Industry Overview and Wood, Plastic, Paper, and Metal Options".

Microwave Susceptor Food Packaging

LU GAO, CHANGFENG GE* and JENNIFER SCHNEIDER
Rochester Institute of Technology, One Memorial Drive, Rochester, NY 14623-5603

ABSTRACT: Microwave susceptor food packaging actively absorbs microwave energy and converts it into heat and makes the food both crisp and brown, while eliminating hot and cold spots. Susceptors are manufactured in the forms of sleeves, bags, pads, trays, cartons, containers, see-through wraps or flexible packaging to meet the different needs of the market. This study reviewed the fundamentals of the microwave susceptor, the featured products and the characteristics that impact performance. The findings suggest that future susceptor food packaging should focus on reducing safety and environmental concerns and use of sustainable packaging materials.

1. INTRODUCTION

MICROWAVE OVENS have been widely used to prepare foods for convenience since the first consumer microwave oven was introduced in 1955 [1]. Nowadays, virtually all American homes, most convenient stores and office kitchens are equipped with microwave ovens [1]. As more people work longer hours and have less time on time-consuming chores, including cooking for themselves in a conventional way, they prefer convenient or ready-to-eat food products. These key factors are driving the growth and developments in microwavable foods rapidly.

According to Mintel International Group Ltd., sales of microwave products, such as frozen pizzas, entrees and snacks, hit $12.5 billion in USA market in 2011 [2]. According to Mintel's Global New Product Database, microwavable refrigerated and frozen products increased by nearly 35% worldwide and 25% in USA from 2005 to 2006 [1–3]. To fully explore the potential of microwave oven, new technologies and innovations have been used in expanding the range of microwave foods and packaging. Milestones in the history of microwave oven are summarized in Table 1 [1,3].

*Author to whom correspondence should be addressed. Email: cfgmet@rit.edu

1557-7244/12/03 149-15

Table 1. Milestones in the History of Microwave Oven [1,3].

1945	Dr. Percy Spencer from the Raytheon Company files a patent for a method of treating food by application of microwave energy for sufficient time to cook the food to a predetermined degree.
1947	First commercial microwave oven introduced by Raytheon for restaurant and institutional use.
1955	First consumer microwave oven introduced.
1967	First countertop domestic microwave oven introduced.
1975	First commercial use of susceptors for pizzas.
1984	First use of susceptors in microwave popcorn applications.

Microwave Heating Mechanisms

Microwaves are a form of electromagnetic energy, different from conventional heating. In conventional heating, foods absorb heat from surrounding hot environment over time. In microwave heating, foods generate heat by their own ingredients or with the help of packaging without the need of a transferring medium, such as hot air, water or oil. Most food heating in a microwave oven is dependent on rapid varying electric field of microwave [4]. Usually it's not important to determine the heating behavior since foods do not interact with magnetic fields, though there is an existing set of magnetic field components. However, some special designed packaging materials can make use of magnetic fields to generate extra heat such as susceptors [3]. Comparison of the temperature gradients of the same food heated in a conventional and microwave oven is shown in Figure 1 [3]. There are three ways for microwave food packaging to react with microwaves: reflecting the ra-

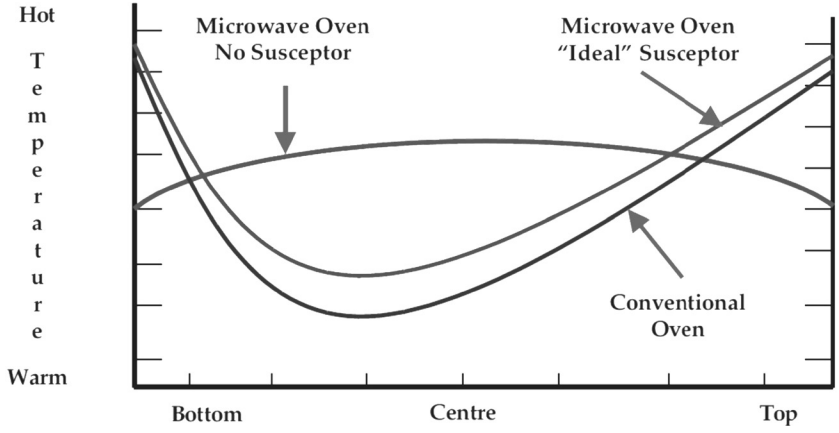

Figure 1. *Temperature gradients in conventional and microwave heating of food [3].*

diation, absorbing the radiation and transmitting the radiation. The heat transfer between food and oven can be influenced by thermal conductivity of the packaging [3].

Microwave Food Packaging

Microwave food packaging is particularly designed for cooking or heating the foods in microwave oven. Microwavable packaging should have all the functions of conventional packaging as well as microwavability. The requirements and performances for microwave food packaging include: (1) Allow microwave cooking or heating quickly; (2) Protect products physically; (3) Have the oxygen, moisture, and microorganisms barrier; (4) Compatibility with contained foods; (5) Evenly cook or heat foods; (6) Keep flavors and aromas in the package during storage and cooking; (7) Be cost effective; (8) Provide for safe opening package after cooking or heating for consumer; and (9) Have an insulated label [4].

Microwave food packaging has evolved from simply containers to something today that boosts the food quality, such as barriers to oxygen, moisture, and flavors [5]. There are two main types of microwave food packaging. One is transparent packaging, referred as microwave passive packaging, which allows microwaves to pass through the package without reacting with it. The other one is absorbent packaging, referred as microwave active packaging, which absorbs microwave energy and converts the energy to heat for cooking or heating the contained food. Microwave active packaging incorporates susceptor, reflector or a guidance system to modify microwaves. There are also other microwave food packaging developed to meet the different product demands, including shielding, field modification, and doneness indicators [3].

2. MICROWAVE SUSCEPTOR FOOD PACKAGING

As stated before, microwave susceptor food packaging also referred as receptor, absorber or heater element, is one type of the microwave packaging. It is made from absorbent materials, which absorb microwave energy and convert that energy into heat to provide extra microwave cooking benefits [3]. This technology combines flexible packaging and thermal processing techniques [6]. Susceptor food packaging crisps, browns and eliminates hot and cold spots of cooked foods, creating the cooked product textures similar to conventional cooking [7].

The first bag of microwave popcorn with microwave susceptor was sold in 1971. It was the metalized film laminated between the layers of paper at the bottom of the bag interacted with microwave energy to hit the temperature of 200°C or higher to get the almost all kernels to pop [5].

Microwave susceptor, consists of a thermally stable and microwave transparent polyester substrate and particles of a metal, such as aluminum or stainless steel, which gives the susceptor a grayish appearance [3,4]. The thickness of an entire susceptor is usually about 10μm and the metal is deposited below 100 nm [8]. There are three methods to deposit or sputter metal (usually aluminum) onto a plastic substrate: vacuum that is commonly used, flake or electron beam [4]. Only aluminum metalized Polyethylene Terephthalate (PET) sheets are for commercial use [9]. This metalized PET film can be adhesively laminated either between two sheets of paper to produce a flexible package, or to paperboard to produce a rigid container, or other rigid materials to provide microwave interactive disposable food packaging [10]. The structure of microwave susceptor for food applications is shown in Figure 2 [9,11]. It consists of four basic layers: (1) Heating surface (usually PET); (2)

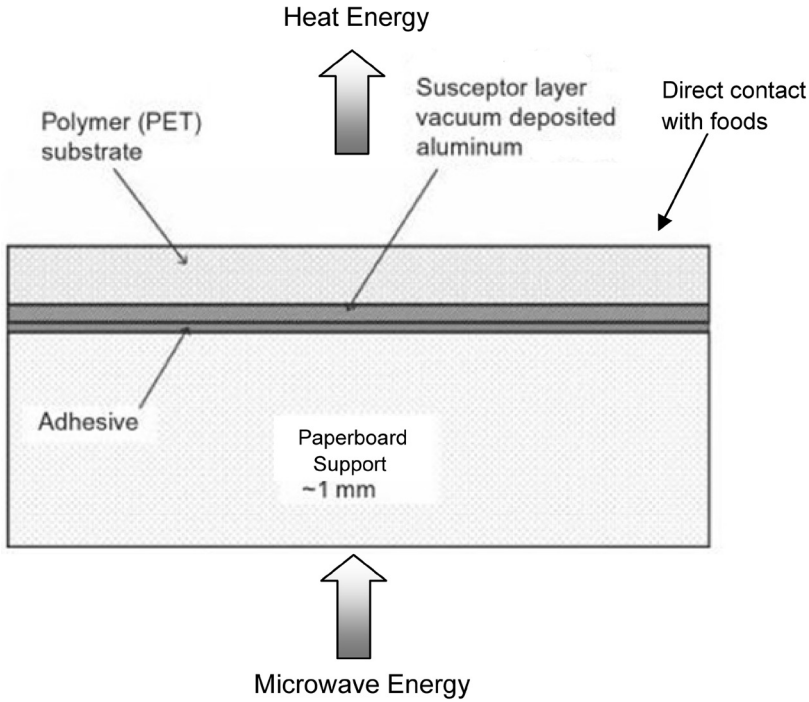

Figure 2. *Layer structure of microwave susceptor for food applications [9,11].*

Thin metal layer (usually vacuum deposited aluminum); (3) Adhesive; and (4) Support structure (usually paper or paperboard) [3].

Susceptors are lossy metal layers to enhance local dissipation of power in a microwave heating [8]. To prevent migration of the metal coating to contained foods and also protect physical or chemical damage of the metal, the metalized side of the susceptor is placed away from the food. As soon as susceptor starts to absorb microwave energy, the thin coating layer breaks up into numerous "islands", which results in a sharp (and essentially irreversible) drop in lossiness until a tolerable power density is reached. After the thin layer breaks up, it limits the maximum temperature. However, the maximum limit is hard to predict or control because it depends on the balance between microwave energy absorption and heat removal. It's important for susceptor contacting with the foods directly to prevent an excessive drop of mass lossiness of metal by having a heat sink to pull heat away from susceptor layer, which makes susceptor operation effective [3].

The fundamental principle of susceptor is to maximize the energy absorption and minimize the reflected and transmitted energy. Surface resistivity, the most important property of the metalized film, is a measure of a thin metal coating's ability to conduct electricity. Starting from zero, the surface resistivity begins to increase as the thickness of the metal is gradually reduced, suggesting all the energy is reflected by the thick metal. Part of the energy is transmitted, and part is absorbed, while less is reflected. As the metal thickness is reduced further, the amount of energy absorbed increases rapidly until it reaches 50% of the incident energy, after which absorption gradually falls to zero while the surface resistivity increases to infinity [3]. This extremely thin layer of aluminum of the susceptor absorbs part of the microwave energy and at the same time creates currents. The currents in the metal are limited due to the very low metal thickness and the resulting high resistivity, which do not cause any arcing or sparking as would be observed with metallic articles in the microwave. However, the currents are high enough to heat the susceptor to a temperature greater than 250 degrees Celsius in only a few seconds and transfer the heat to contained products [12], as shown in Table 2 [3].

However, with all the advances, one issue still exists with the metalized whole surface application or the non-patterned (conventional) susceptors. Conventional susceptors are limited in their size capability, and cannot brown or crisp the center of the product as expected. For example, a frozen microwave packaged pizza in 7 inches diam-

Table 2. Maximum Interface Temperatures between Product and Susceptor [3].

Product	Maximum Temperature (°C)	Heating Time (sec)	Comments
Susceptor alone	316	100	No food load
Popcorn	247	150	Normal
Popcorn	280	220	Extended heating
Fish fillet	222	290	Not turned
Pizza	223	290	Not turned

eter, the susceptor in connection with the pizza browns and crisps the crust of the pizza well as the oven baked pizza. However, if the pizza size is between 8 to 12 inches diameter, the conventional susceptor cannot brown or crisp the center of the pizza satisfactorily. Patterned microwave susceptor is designed to meet the demand of the specific food product. More heating energy can be directly delivered to targeted heating locations on the food. A great variety of microwave susceptors in different patterns developed to satisfy different product needs have been patented. There are four methods to produce patterned metalized susceptors, which are pattern demoralization, hot stamp transfer, hot nip transfer, and film to film transfer.

Many other factors also affect the performance of microwave susceptor packaging, such as frequency of the microwaves, product characteristics, thickness and evenness of the deposited metal, and physical characteristics etc. Product characteristics include product shape, density, size, salt content, minerals, amount of free and bound water, product species and composition. High salt content foods are easier to be heated in high temperature than low salt content foods [4]. Holes and crack in the susceptor surface, and the change in the crystallinity of PET film are also the reasons to reduce the susceptor heating ability. The dimension, shape and material of construction of packages can alter the way of heating the contained foods too.

There are various applications for using microwave susceptor food packaging technology to avoid microwave-prepared foods to be “too soggy” or “too many cold spots” [13]. Over the past couple of years, different combinations of metal depositing and plastic films have been explored for better microwave effect. There are some new types of susceptors emerging, beyond the metalized film susceptors, such as printed ink systems, and modified ceramic susceptors, etc. [14]. These alternatives have yet to be commercialized with new product applications.

Susceptors are manufactured as sleeves, bags, pads, trays, cartons, containers, see-through wraps or flexible packaging [4]. Sleeve is constructed of paper or paperboard laminated to metalized microwave susceptor film, using to crisp and brown food wrapped inside in a microwave oven [Figure 3(a)] [15]. It can be customized to have vents, open zippers, gussets. Pad can be used where the bottom of a product needs to be crisped or browned while the top does not need additional heat [Figure 3(b)] [16]. It can be die-cut to match the product size. It has both non-patterned and patterned for specific needs. Microwave popcorn bag is a designed paper bag with susceptor laminated on one side to absorb microwaves and get additional heat at the film interface and distributes the heat inside of the bag to pop kernels evenly [Figure 3(c)]. Microwave popcorn also can be packaged in heat seal carton with susceptor at the bottom.

Applications of microwave susceptor packaging may include: Microwave Popcorn, Microwave Hot Sandwiches, Microwave Baguettes, Microwave Pizza Snacks, Microwave Paninis, Microwave Pizza, Microwave Sausage Rolls, Microwave Pastries, Microwave French Fries, Frozen Entrées, and Frozen Sea foods.

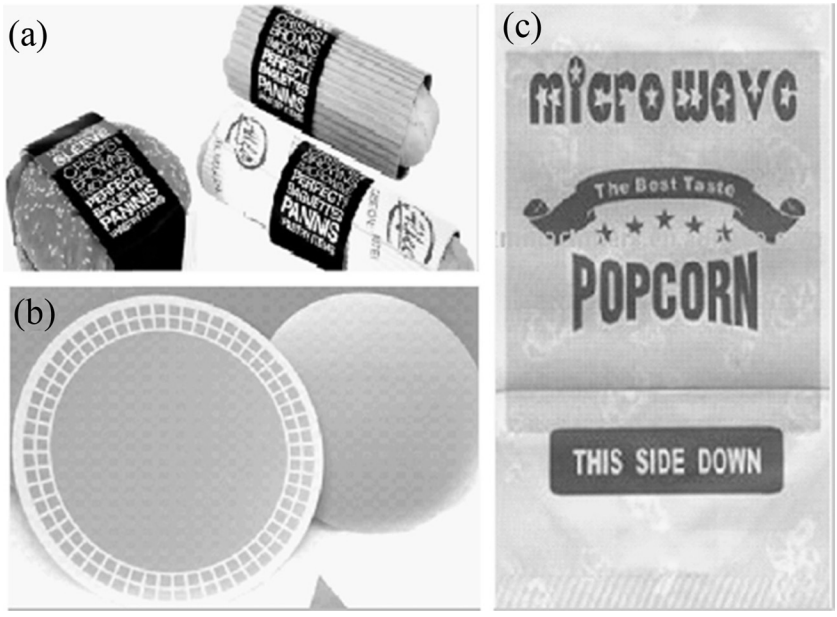

Figure 3. *Examples of microwave susceptor food packaging. (a) Microwave susceptor sleeves, (b) Microwave susceptor pads, (c) Microwave susceptor popcorn bag.*

3. FEATURED MICROWAVE SUSCEPTOR FOOD PACKAGING

Due to consumer demand for high quality, quick foods, the market for susceptor packaging will continue to grow. Therefore, many manufacturers have responded with different applications to meet this market. Below is an abbreviated summary of the range of susceptor packing options on the market:

Featured Products by Exopack-Technology LLC

Insta-Bowl™—a laminated bag, constructed of two grease-proof, paper plies with a microwave susceptor patch trapped between them [Figure 4(a)] [17]. A pull-string easy open feature releases the top seal of the package, and its triangular shape allows it to sit flat and form a shallow, ready-to-eat bowl. It is an award-winning bag-and-bowl microwave popcorn packaging product, targeted to vending machine, convenience-store customers or new portion control branded products. Insta-Bowl™ won an AmeriStar Award from the Institute of Packaging Professionals in 2004. This package also was a multiple Flexible Packaging Association Award winner in 2005, a Gold Award for technical innovation and a Silver Award for packaging excellence [17].

Crispi-Wrap™—a microwave susceptor laminated between two paper plies with venting apertures, which is able to evenly cooked or heated product with improved crisping and browning. It is designed for egg rolls, burritos, chimichangas, calzones, and much more [17].

Featured Products by Graphic Packaging International Inc.

QwikCrisp®—Cartons, sleeves and trays designed to brown and crisp bread and dough-based products, perfect for snacks, appetizers, pizzas, and sandwiches [18]. One example is Hot Pockets® from Nestlé, the hand-held sandwich-snack and the first microwavable food to break the crisping barrier [Figure 4(b)] [18]. Examples include DiGiorno Microwave Rising Crust Pizza and DiGiorno Microwave Thin Crispy Crust Pizza introduced by Nestlé in 2004. The packaging of DiGiorno Microwave Rising Crust Pizza includes a modified atmosphere pouch (MAP), which the consumer removes before cooking. The pouch is tucked into a tray, which, when turned upside down, becomes a cooking platform for the product. The cooking surface is a paperboard/susceptor lami-

Figure 4. *Featured microwave susceptor food packaging products. (a) Insta-Bowl™ microwave popcorn, (b) Hot Pockets® frozen stuffed hand-held sandwiches, (c) DiGiorno microwave rising crust pizza and DiGiorno microwave thin crispy crust pizza, (d) Oscar Mayer Fast Franks, (e) Ore-Ida's extra crispy easy golden fries, (f) Coneinn pizza cone packed in cone shape sleeve, (g) POPZ microwave popcorn packed in Heat Seal Carton, (h) Smart Pouch® for Delitefuls™ mango tango tilapia, (i) Aldi Private-Label frozen entrees, (j) Sira-Crisp™ Crisp-it™ microwave susceptor films.*

nate. There is a crisping ring to cover the exposed crust. The susceptor of the tray and the ring direct the microwave energy throughout the pizza so the crust rises and the toppings cook evenly. The ring makes the exterior crispy and keeps inside soft and tender. The packaging of DiGiorno Microwave Thin Crispy Crust Pizza does not have a crisping ring. The tray is die cut with circular holes as well as a pattern of slits to ensure proper cooking [Figure 4(c)] [13].

Microflex®—designed to brown and crisp dough-based products like snacks, appetizers, pizzas, sandwiches in flexible pouches, bags, roll-stock, lidding material and patches [18].

Quiltwave™—a flexible, three-layer, active microwave food package. It is a combination of paper, plastic and metal. Light paper is laminated on both sides with PET film to brown and crisp irregularly shaped products such as burritos, egg rolls, hotdogs, wraps in flexible packaging [18]. Moisture naturally trapped between the layers creates pockets or bubbles in the substrate. When the designed laminated cells, or 'quilts', expand, inflated cells touch the surface of the food and insulate it from the environment to increase sensible heat flux to the food surface, which causes maximum browning and crisping. During this time, channels between the inflated cells allow moisture to evaporate from the food's surface and out of the package, enhancing crisping. Once the food cooked, the cells remain inflated to protect the consumer from hot food inside when the package cools. Quiltwave™ was awarded the prestigious 'Best of the Best' Dupont Award for innovative Packaging for 2005. It also won the AmeriStar Award from the Institute of Packaging Professionals (IoPP). The Quiltwave™ package is ideal for convenience foods [19]. Oscar Mayer Fast Franks from Kraft Foods is America's favorite hot dog from vending machine [Figure 4(d)] [20]. The packaging comes with a susceptor tray that heats the bun evenly and makes it soft and delicious [20]. Sepps Microwavable Grilled Cheese, from Sepps Gourmet Foods, was introduced on the market in 2005. It is North America's first microwavable grilled cheese sandwich. The packaging of Sepps Microwavable Grilled Cheese uses Graphic Packaging International (GPI)'s patented microwavable packaging technology Quiltwave™. In order to brown and control the moisture in the middle of the sandwich, Quiltwave™ sleeve shrinks down over top of the middle part while not overcooking the crust [21].

MicroRite™—Trays, bowls, sleeves and discs that provide thoroughly even heating for large entrées. Ideal for frozen meals, larger pizzas, sandwiches, soups [18]. Cape Cod Cuisine products, from Raw

Sea Foods Inc., use MicroRite Even Heating trays. The tray is an aluminum foil pattern laminated to a paperboard substrate [7]. Wal-Mart's 40-oz. lasagna is packaged in paperboard Micro-Rite tray, which is the first product to launch nationally in the MicroRite tray within the U.S. President's Choice frozen fruit pies packed in MicroRite package debuted in Canadian supermarkets in Nov, 2003. The pie plate is made of metalized polyester, which browns and crisps, and metallic foil that channels microwave energy to desired areas of oven and energy [22].

DesignerWare™—Attractive pressed paperboard trays replace nonrenewable plastic trays. Outside surface allows for high-impact graphics, reducing packaging needs. It is great for frozen meals, pasta, entrées, and salads [18]. Ore-Ida's Extra Crispy Easy Golden Fries® from Heinz Co. uses dual-susceptor packaging developed from GPI [Figure 4(e)] [23] .

Featured Products by Inline Packaging LLC

Superceptor™—supercharges the heat output of a conventional metalized susceptor for foods that are difficult to crisp such as pizzas, eggrolls, and sandwiches. Superceptor™ can increase heat in demand areas such as the center of a pizza or the middle of an eggroll, compared to conventional susceptors having just one temperature output [16].

Micro~Grill™—converts an ordinary microwave into a convenient and quick Panini grill. It incorporates performance enhancing features unachievable with standard single ply or corrugated susceptors. These include: focused energy pattern for enhanced grill lines, vertical and horizontal moisture vent channels, increased susceptor heat output, and multiple paperboard layers for rigidity and moisture resistance [16].

Susceptor Sleeve—metalized microwave susceptor film laminated to paper or paperboard. To meet customer needs, it can have vents, opening zippers, or gussets. It is perfect for handhold foods such as eggrolls, wraps, enchiladas, corn dogs, etc. Coneinn Pizza Cone is made of cone shaped susceptor sleeve with multiple temperature zones as well as venting [Figure 4(f)] [16]. The easy opening allows the consumer to tear away the top of the sleeve, but still leaving a hold for convenience [16].

Heat Seal Carton—designed for high temperature application but the heat seal should not be contacted with foods, such as microwave popcorn and other food products. POPZ microwave popcorn [Figure 4(g)] [16] consists of 17-point solid bleached sulfate (SBS) base adhesive-laminated to a high barrier aluminum-oxide-coated polyester equipped

with a demetalized Camcrisp susceptor manufactured by Amcor Flexibles-Camvac, U.K [16].

Featured Products by Smart Pouch LLC

Smart Pouch® Technology—has three issued U.S. patents and a new patent pending. It incorporates susceptor into the structure of steam pouches and has the benefits of both steam and susceptor technology, which allows consumers to cook raw frozen protein entrees in the microwave oven and have the similar cooking results as conventional cooking. Smart Pouch® packaging is designed for the cooking or reheating of frozen protein entrees and portions. Meat proteins (seafood, poultry, pork and beef) need higher temperatures than boiling water and steam (212°F at sea level) to have tender texture [24]. Susceptor not only increases the temperature to cook through the protein, also with steam environment the meat will not be dry out or be rubbery. The pouch material is dual-ovenable, so cooking can take place in either the microwave oven or multiple pouches in a conventional oven [6]. The application Smart Pouch® can range from a simple protein portion to a complete entree, for example:

- Delitefuls™ Mango Tango Tilapia includes two individual Smart Pouch® bags [Figure 4(h)] [24]. For product particular application, this packaging has patterned metalized aluminum laminated between PET and paper [24].
- Aldi grocery retailer launched its private-label six frozen new entrees [Figure 4(i)] [6], which are packaged in form-fill-seal (FFS) pouches made by Smart Pouch LLC and Graphic Packaging International (GPI). The flexible packaging materials incorporate steam cooking and patterned microwave susceptors between layers of PET and kraft paper [6].

Featured Products by Vacumet Metalized Plastic

Barrier-Met® Susceptor Polyester—a balanced, oriented polyester film metalized on one side and corona treated on the other. To meet different consumer demands, Barrier-Met® Susceptor Polyester is made by controlling optical density (parameter used for the characterization of the metallic layer thickness) of metalized aluminum in a tight range of ± 0.03 [25].

Featured Products by Sirane Ltd

Sira-Crisp™ Crisp-it™—lightweight susceptor packaging, ideal for the travel industry, convenience and retail sector [Figure 4(j)] [26]. This crisp film can be combined with other packaging materials to make a variety of microwave susceptor products for different purposes. For example, *Sira-Cook™ Crisp-it Dry™* - Sira-Cook™ Crisp-it product with an absorbent layer underneath, specially designed to crisp-up dough and pastry-based foods in the microwave, such as paninis, pizzas, sausage rolls and pasties, as well as potato wedges, chips and popcorn [26].

Featured Products by BCP Fluted Packaging Ltd

Discs (for pizza)—Fluted or flat Susceptor can be produced.

Crisping Sleeves —For hot sandwiches, baguettes, paninis, sausage rolls, pasties and more [15].

Featured Products by Camvac Limited

Camcrisp®—Low optical density metalized films for microwave susceptors. It's designed for microwave snack market, such as such as pizzas, garlic bread, potato chips and popcorn [27].

As all the featured products we discussed here, the main benefits of these susceptors are crisping and browning, though their ability to increase temperatures by focusing electromagnetic energy and causing greater friction of charged molecules is a functional advantage [2]. It is hard to determine if one product(s) is better than the others since each of them has different features. For example, fully metallized film produces one heat output and is prone to undercooking the center and overcooking the edges of food. Demetallized film reduces the likelihood of overcooking but results in less browning and relatively low heat. Printed susceptors are prone to runaway heating.

4. FUTURE OF MICROWAVE SUSCEPTOR FOOD PACKAGING

Microwave convenience foods are changing people's lifestyle and economy. The invention of susceptor packaging extends the range of microwave foods and boosts the quality of microwave cooking. However, there are some safety concerns on microwave susceptor food packaging.

A major concern is the migration of unknown compound from susceptor to the food and whether there are any volatiles released from adhesive in high cooking temperatures. The food and packaging industries are conducting extensive research. One project showed that for a specific product, popcorn, there was no transfer into the food [29]. Work is continuing to validate methods to test for non-volatile compounds. Another issue is that microwave susceptor packaging cannot be reused for heating or cooking foods. The reason is that the adhesive between susceptor and the support material may be damaged in the original use [29,30]. If reheated again, any packaging material is possible to migrate into the food. Also after first time heating, susceptor usually loses its ability to absorb microwave energy safely. If reheated again, any change in susceptor may cause it burn [5]. Last concern is susceptor does heat up to around 250°C, but the packaging material may scorch if there is no food direct contact with susceptor [10]. In order to efficiently and properly use susceptors in the microwave field, evaluation of susceptor condition should be done before use.

5. CONCLUSIONS

Today microwave susceptor food packaging plays an important role in microwave food packaging. The new trends of susceptor packaging include: Improve the quality and convenience of microwavable foods by innovations in microwave susceptor food packaging [3]; Reduce the potential consumer safety and environmental concerns; Improve uniform heating [3]; and Develop sustainability of packaging materials [5]. Sustainability of packaging materials is one of the largest concerns in the packaging industry. Many companies and organizations have invested considerable research to understand and address sustainability, such as the Sustainable Packaging Coalition in the United States and the Sustainable Packaging Alliance in Australia. Both bio-based and bio-degradable materials are being investigated as potential packaging materials. A full discussion on sustainability, however, is beyond the scope of this paper.

REFERENCES

1. Gallawa, J.C., 1998. The history of the microwave oven, Available: http://www.gallawa.com/microtech/history.html.
2. Higgins, K.T., Susceptors and the safety challenge, Available: http://www.foodengineeringmag.com/articles/susceptors-and-the-safety-challenge.

3. Robertson, G., 2005. *Food Packaging: Principles and Practice,* Boca Raton, FL: CRC Press.
4. Micro-Ovenable Packages and Retortable Packages, Available: http://icpe.in/icpefoodnpackaging/pdfs/27_microovenable.pdf.
5. Risch, S., Food Packaging History and Innovations. J*ournal of Agricultural and Food Chemistry,* 2009, 57(18), pp. 8089-8092.
6. Connolly, K.B., Flexible Packaging Takes the Heat, 2011, Available: http://www.foodprocessing.com/articles/2010/flexible-packaging.html.
7. Bertrand, K., Thinking inside the box, carton and tray. 2005, Available: http://www.foodprocessing.com/articles/2005/491.html.
8. Celuch, M., Gwarek, W. and Soltysiak, M., Effective modeling of microwave heating scenarios including susceptors, *Proceedings of International Conference on Microwave,* 2008, 08, November 21–24.
9. Česnek, J., Dobiáš, J., Houšová, J. and Sedláček, J., Properties of Thin Metallic Films for Microwave Susceptors, *Czech J. Food Sci.,* 2003, 21(01), pp. 34–40.
10. Risch, S., 2000. *Food Packaging: Testing Methods and Applications (ACS Symposium),* American Chemical Society.
11. Mehdizadeh, M., 2010. *Microwave/RF Applicators and Probes for Material Heating, Sensing, and Plasma Generation: A Design Guide.,* Oxford, UK. William Andrew.
12. VAST Microwave Susceptors, Available: http://www.vastfilm.com/index_files/Page1204.htm.
13. Pehanich, M. and Fusaro, D., Susceptors enable a new generation of microwave foods. 2005, Available: http://www.foodprocessing.com/articles/2005/234.html.
14. Labuza, T. & Meister, J., An Alternate Method for Measuring the Heating Potential of Microwave Susceptor Films. *J. International Microwave Power and Electromagnetic Energy,* 1992, 27 (4), pp.205–208.
15. BCP's Susceptor, Availble: http://www.bcpflute.com/microwave-susceptor/.
16. Innovative Microwave Packaging, Available: http://www.inlinepkg.com/.
17. Insta-Bowl™, Available: http://www.exopack.com/prod_instabowl.php.
18. Microwave packaging satisfies more with quick and tasty cooking. Available: http://www.graphicpkg.com/innovation/pages/microwavepackagingsolutions.aspx.
19. Food Packaging: Package converts microwave into baking oven. 2003, Available: http://www.foodengineeringmag.com/Articles/Column/26215103942f8010VgnVCM100000f932a8c0.
20. Microwave Packaging Wins Consumers For Oscar Mayer and Ameristar Award For Graphic Packaging, Available: http://phx.corporate-ir.net/phoenix.zhtml?c=103159&p=irol-newsArticle_pf&ID=1177161&highlight=.
21. Sepp's Quilt Wave Microwave Packaging Technology, 2004, Available: http://www.packaging-gateway.com/projects/sepp.
22. Connolly, K.B., For Which Oven? 2008, Available: http://www.foodprocessing.com/articles/2008/086.html?page=2.
23. Bertrand, K., Microwavable Foods Satisfy Need for Speed and Palatability, Food Technology, Vol. 59, No.1, 2005.
24. Smart Pouch®, Available: http://www.smartpouch.com/how_it_works.html.
25. Barrier-Met® Susceptor Polyester, Available: http://www.vacumet.com/metallized-plastic-applications/microwave-susceptor/.
26. Sira-Crisp™ Crisp-it™, Available: http://www.sirane.com/divisions/food-packaging.html.
27. Camcrisp®, Available: http://www.camvaclimited.com/product.aspx?id=3.
28. Food Packaging: Is it safe to re-use food packaging materials? 2011, Available: http://extension.psu.edu/food-safety/food-preservation/faq/food-packaging.
29. Risch, S., Safety assessment of microwave susceptors and other high temperature packaging materials, *Food additives and contaminants,* 1993, 10(6), pp. 655–661.
30. The safety of microwave ovens, 2009, Available: http://www.csiro.au/en/Outcomes/Food-and-Agriculture/safety-of-microwave-ovens.aspx.

Migration Model of Chemical Substances from Paper-plastic Packaging Material into Food

XIULING HUANG[1,*], JUN WANG[2], YALI TANG[1], YONG ZHU[3,4] and ZHIWEI WANG[3,4*]

[1]*School of Mechatronics Engineering and Automation, Shanghai University, Shanghai 200072, PRC*

[2]*Department of Packaging Engineering, Jiangnan University, Wuxi 214122, PRC*

[3]*Packaging Engineering Institute, Jinan University, Zhuhai 519070, PRC*

[4]*Key Laboratory of Product Packaging and Logistics of Guangdong Higher Education Institues, Jinan University, Zhuhai 519070, PRC*

ABSTRACT: Paper or recycled paper containing contaminant can be used for food packaging if the food is protected by a functional barrier made of plastic coating. The problem of contaminant transfer through the packaging was studied from a theoretical viewpoint. A migration model was built to provde predictions of concentration and amount of contaminant. The equations were built based on *Fickian* diffusion, and analytical solutions were obtained through Laplace transformation and inversion theorem. Different diffusivities of contaminant in the two layers and partition coefficient k_{CP} at the interface of paper and plastic coating were considered in the model The effects of k_{CP}, thicknesses of paper and plastic coating on the migration were discussed. In addition, the applicability of the model as bi-layer polymer packaging was also studied. The effects of concentration and $L\cdot(L + H)^{-1}$ (thickness ratio of paper and packaging) on migration were analyzed. The model obtained can be used universally for other types of bi-layer packaging materials such as for two plastic combinations.

1. INTRODUCTION

PAPER and paperboard materials are widely used as food-packaging materials and packaging containers such as boxes, bowls, cups, etc. Reclaimed fiber is also used in some paper or paperboard food packaging materials. The US Food and Drug Administration (FDA) promulgated a food additive regulation to allow the use of pulp from reclaimed

*Authors to whom correspondence should be addressed. E-mail: xiulh@shu.edu.cn, wangzw@jnu.edu.cn

1557-7244/12/03 165-19

fiber in food packaging [1]. However, many chemical substances such as defoamers, pesticides, optical brighteners, biocides and printing pigments may be intentionally added during the initial production, and become unintentional additives components when recycled. There is thus the potential for migration of these substances into food and subsequent contamination. The migration of chemical substances from paper or paperboard into food has indeed happened [2–7], which can be a risk to public health. To reduce migration from paper packaging, a protective plastic coating layer such as polyethylene (PE) or polypropylene (PP) is applied on the surface of food packaging. The plastic coating layer plays the role of a functional barrier which is able to protect the food from contamination for some time. The migration of contaminants from paper or paperboard through plastic coating has also been studied by several researchers [8–11].

Recently, the experimental research in this area has started, but the theoretical research is still deficient. Modeling of migration of contaminants from a recycled polymer through a virgin polymer layer, namely, a bi-layer polymer packaging, have been studied in previous research [12–18], and a few books have clearly described the mathematical treatment of mass transfer by diffusion [19,20], which all consider the identical diffusivity in both layers. However, the different diffusivity in the two layers and the partition coefficient at the interface of two polymer layers had not been considered. In fact, the problem of diffusion in paper-plastic coating materials in contact with food is more complex than bi-layer polymer materials.

The objective of this study is to develop a theoretical model of mass transfer through a bi-layer packaging system consisting of paper-plastic coating into food. Unidirectional transfer, different diffusivities of contaminants in paper and plastic coating, and partition coefficient at the interface between paper and plastic coating are considered. A series of analytical solutions are obtained. Factors which affect contaminants concentration in paper and plastic coating and migration amount in plastic coating and food are discussed. The model will also be applied universally, not only to paper-plastic coating bi-layer system, but also to polymer-polymer bi-layer packaging system.

2. THEORETICAL MODELING

The problem of diffusion for paper-plastic coating of packaging is highly complex, the following assumptions are made in order to make

the process analyzed clearly regarding limited packaging and unlimited food.

2.1. Assumptions

The principal assumptions for model development are as follows: (1) The packaging material consists of two layers in perfect contact. One is a paper with contaminants in it, while the other is a virgin plastic coating as shown in Figure 1; (2) The contaminant is initially in the paper at a uniform concentration, while the plastic coating is free from contamination; (3) The contaminant migrates through paper and plastic coating layers and through the interface between the food and plastic coating with an infinite coefficient of mass transfer. There is no transfer of contaminant through the external surface of the paper in contact with air; (4) The transfer of a contaminant through the paper and plastic coating is controlled by *Fickian* diffusion with constant diffusivities, which are D_P for paper and D_C for plastic coating respectively; (5) The partition coefficient, k_{CP}, of a contaminant is constant at the interface of paper and plastic coating; (6) There is no transfer of food to the packaging; (7) The partition factor of the contaminant is taken as 1 at the interface of packaging and food; (8) The sorption of a contaminant by paper is negligible.

2.2. Mathematical Treatment

The one-dimensional diffusion through the packaging is expressed by *Fick*'s equation with constant diffusivities in the paper and in the plastic coating.

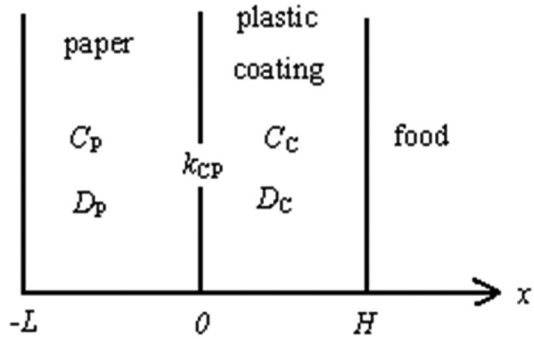

Figure 1. *Scheme of the package-food system.*

$$\frac{\partial C_P(x,t)}{\partial t} = D_P \frac{\partial^2 C_P(x,t)}{\partial x^2} \qquad (-L < x < 0) \tag{1}$$

$$\frac{\partial C_C(x,t)}{\partial t} = D_C \frac{\partial^2 C_C(x,t)}{\partial x^2} \qquad (0 < x < H) \tag{2}$$

where $C_P(x,t)$ and $C_C(x,t)$ are the concentrations of contaminant in paper and plastic coating, respectively, at position x and time t, D_P and D_C are the constant diffusivities of contaminant in paper and plastic coating, respectively, and L and H are the thickness of paper and plastic coating, respectively.

The initial conditions are

$$t = 0 \quad -L < x < 0 \quad C_P = C_{P0} \tag{3}$$

$$0 < x < H \quad C_C = 0 \tag{4}$$

where C_{P0} is the initial concentration of contaminant in paper.

The boundary conditions express the fact that there is no external transfer at $x = -L$, the flux of contaminant is continuous whereas the concentration itself is discontinuous at $x = 0$.

$$t > 0 \quad x = -L \quad \frac{\partial C_P}{\partial x} = 0 \tag{5}$$

$$x = 0 \quad D_P \frac{\partial C_P(x,t)}{\partial x} = D_C \frac{\partial C_C(x,t)}{\partial x} \tag{6}$$

$$x = 0 \quad C_C = k_{CP} C_P \tag{7}$$

$$x = H \quad C_C = 0 \tag{8}$$

where k_{CP} is the constant partition coefficient of contaminant at the interface of plastic coating and paper. $C_C = 0$ just because the amount of contaminant migrating into food with respect to the amount of food is small.

Laplace transformation, inversion theorem, residues theorem and simplification were applied to solve Equations (1) and (2) to get the

concentrations C_P and C_C under the initial and boundary conditions. The solutions are as follows:

$$C_P = 2C_{P0}k_{CP}\sum_{n=1}^{\infty}\frac{\sin(\beta_n L)\cos^2(\alpha\beta_n H)\cos[\beta_n(x+L)]}{\beta_n[k_{CP}L\cos^2(\alpha\beta_n H)+\alpha^2 H\sin^2(L\beta_n)]}e^{-D_P\beta_n^2 t} \tag{9}$$

$$C_C = 2C_{P0}k_{CP}\sum_{n=1}^{\infty}\frac{\sin^2(\beta_n L)\cos(\alpha\beta_n H)\sin[\beta_n(H-x)]}{\beta_n\left[\frac{k_{CP}L}{\alpha}\cos^2(\alpha\beta_n H)+\alpha H\sin^2(\beta_n L)\right]]}e^{-D_P\beta_n^2 t} \tag{10}$$

where,

$$\alpha = \sqrt{\frac{D_P}{D_C}}$$

(n = 1, 2, 3, . . .) are the positive roots of Equation (11)

$$k_{CP}\cot\beta L - \alpha\tan\alpha\beta H = 0 \tag{11}$$

M_{Ct} and M_{Ft} are obtained according to definition

$$M_{Ct} = \int_0^H C_c(x,t)dx =$$
$$2k_{CP}C_{P0}\sum_{n=1}^{\infty}\frac{[1-\cos(\alpha\beta_n H)]\sin^2(\beta_n L)\cos(\alpha\beta_n H)}{\beta_n^2[k_{CP}L\cos^2(\alpha\beta_n H)+\alpha^2 H\sin^2(\beta_n L)]}e^{-D_P\beta_n^2 t} \tag{12}$$

$$M_{Ft} = \int_0^t AJ_H dt = \int_0^t A(-D_C\frac{\partial C_C}{\partial x}|_H)dt =$$
$$-2AC_{\mathrm{p0}}k_{CP}\sum_{n=1}^{\infty}\frac{\sin^2(\beta_n L)\cos(\alpha\beta_n H)}{\beta_n^2[k_{CP}L\cos^2(\alpha\beta_n H)+\alpha^2 H\sin^2(\beta_n L)]}(e^{-D_{\mathrm{p}}\beta_n^2 t}-1) \tag{13}$$

where A is the area, J is the flux, M_{Ct} is the amount of contaminant in plastic coating layer, and M_{Ft} is the amount of contaminant in food.

3. RESULTS AND DISCUSSIONS

This model is applied to two kinds of bi-layer packaging systems: a paper-plastic coating system and a polymer-polymer system.

3.1. Paper-Plastic Coating Bi-layer Packaging System

For food packaging systems consisting of paper-plastic coating layer, the results are expressed in three ways: (1) the transfer kinetics of contaminant into plastic coating and food for various k_{CP}; (2) the profiles of contaminant concentration for various k_{CP}; and (3) the transfer kinetics of contaminant into plastic coating and food for various thicknesses of paper or plastic coating.

3.1.1. Transfer Kinetics of Contaminant into Plastic Coating and Profiles of Contaminant Concentration through the Packaging for Various Values of k_{CP}

The definition of k_{CP} is the ratio of concentration of contaminant in plastic coating to the concentration of the contaminant in paper at migration equilibrium. The transfer kinetics and the concentration profiles were calculated using Equations (9), (10) and (12), (13). The diffusivities D_P and D_C are 10^{-4} and 10^{-8}, respectively which are the practical values. The curves drawn are shown in Figure 2 to Figure 5 for various values of k_{CP}. From these curves the following conclusions can be drawn about the influences of the partition coefficient at the interface of paper and plastic coating.

1. The amount of contaminant in plastic coating and food increase with k_{CP} as shown in Figure 2 and Figure 3. This phenomenon can be explained based on the definition of k_{CP}.
2. The concentration profiles are drawn using the dimensionless numbers $C \cdot C_{P0}^{-1}$, with various values of k_{CP} ranging from 0.2 to 0.6, and different thickness of paper and plastic coating. The curves are shown in Figure 4 and Figure 5. According to Figure 4 and Figure 5, the concentration of contaminant in paper remains almost the same at the beginning of the process when the thicknesses of paper and plastic coating are identical. However, the concentration of the contaminant in paper decreases at the beginning of the process when the thickness of paper is much thicker than that of plastic

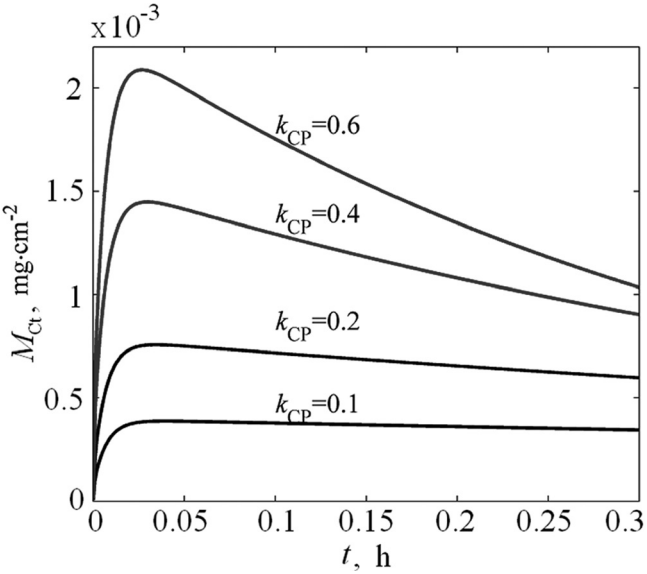

Figure 2. *Transfer kinetics of contaminant into plastic coating for various values of k_{CP}, (L = 48 μm, H = 16 μm, C_{P0} = 5 mg·cm^{-3}).*

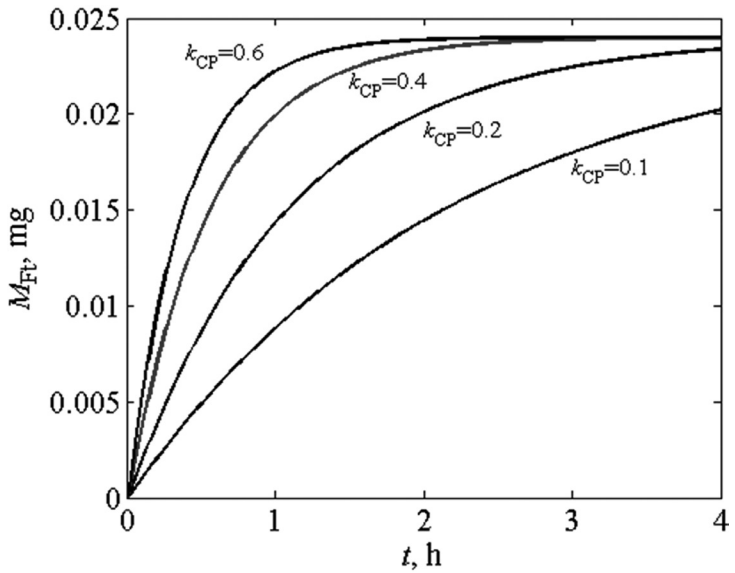

Figure 3. *Transfer kinetics of contaminant into food for various values of k_{CP}, (L = 48 μm, H = 16 μm, A = 1 cm^2, C_{P0} = 5 mg·cm^{-3}).*

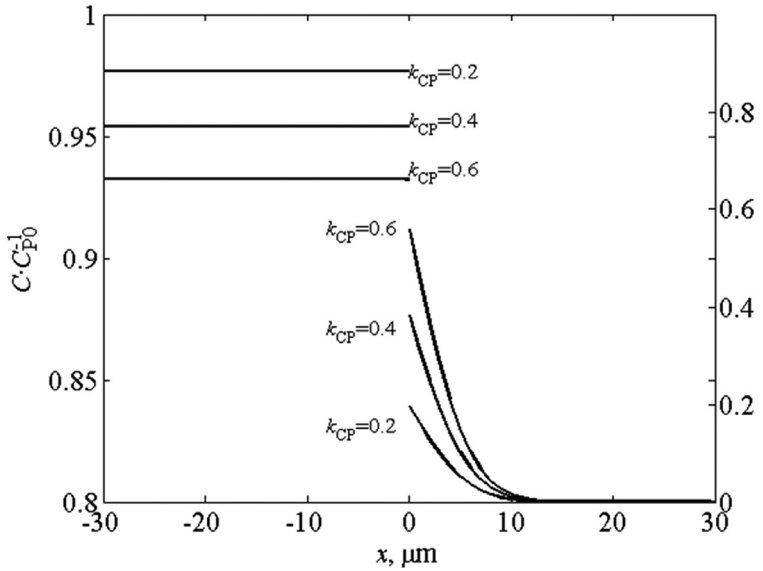

Figure 4. *Profiles of contaminant concentration through the packaging for various values of k_{CP}, (L = 30 μm, t = 10 s).*

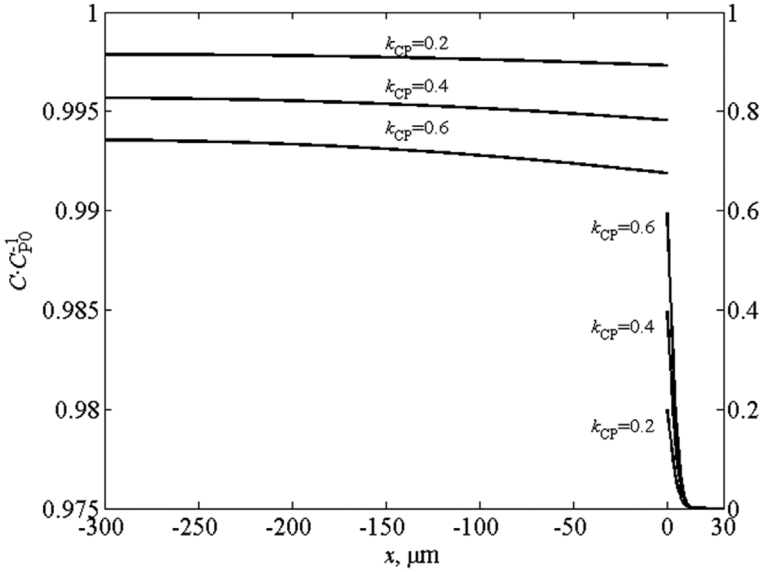

Figure 5. *Profiles of contaminant concentration through the packaging for various value of k_{CP}, (L = 300 μm, H = 30 μm, t = 10 s).*

coating. It can be concluded that the thicker the paper relative to the plastic coating, the less the food can be effectively protected.

3.1.2. Transfer Kinetics of Contaminant into Plastic Coating and Food for Various Thicknesses of Paper and Plastic Coating

In order to understand the effect of thickness, it is necessary to study the transfer kinetics of contaminant for various thicknesses of paper and plastic coating. The transfer kinetics graphs are shown in Figure 6 to Figure 9. The amounts of contaminant in plastic coating and food are expressed in terms of time. The conclusions drawn from the graphs are as follows:

1. When the initial concentration of contaminant in paper, the value of k_{CP} and the thickness of plastic coating are constant, the amount of contaminant migrating into plastic coating and food increase obviously with the increase of the thickness of paper as shown in Figure 6 and Figure 7. Thus, for the same initial concentration of contaminant in paper, thicker paper contains a higher amount of contaminant in paper.

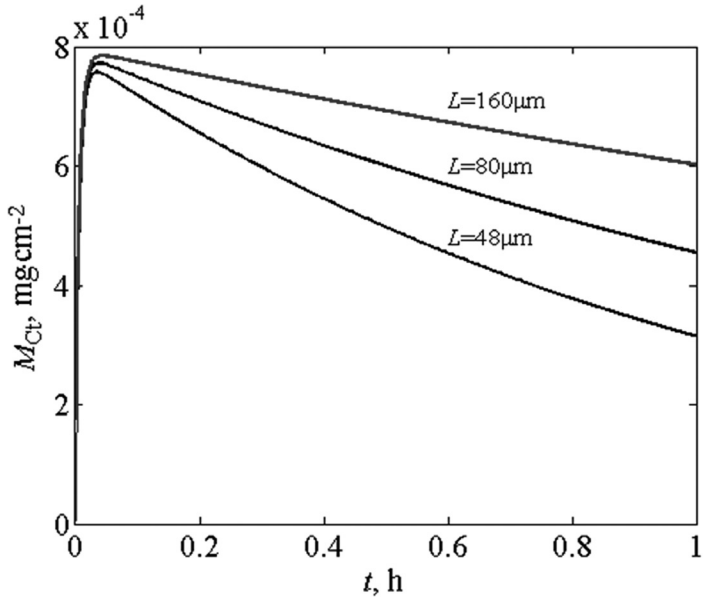

Figure 6. *Transfer kinetics of contaminant into plastic coating for various thickness of paper, (H = 16 μm, C_{P0} = 5 mg·cm^{-3}, k_{CP} = 0.2).*

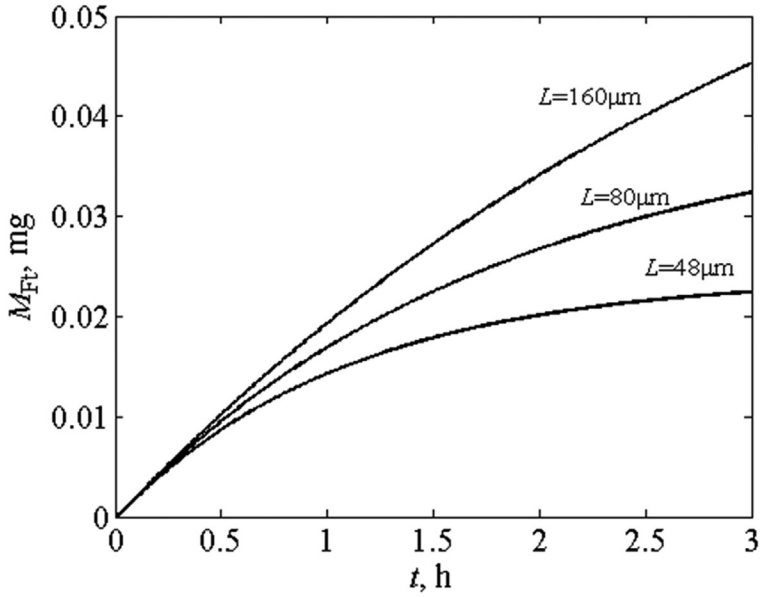

Figure 7. *Transfer kinetics of contaminant into food for various thickness of paper, (H = 16 μm, A = 1 cm^2, C_{P0} = 5 mg·cm^{-3}, k_{CP} = 0.2).*

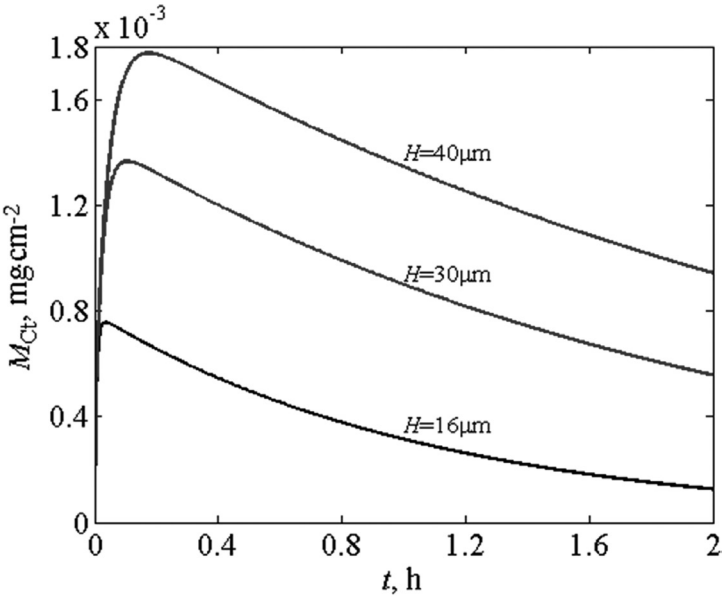

Figure 8. *Transfer kinetics of contaminant into food for various thickness of plastic coating, (L = 48 μm, C_{P0} = 5 mg·cm^{-3}, k_{CP} = 0.2).*

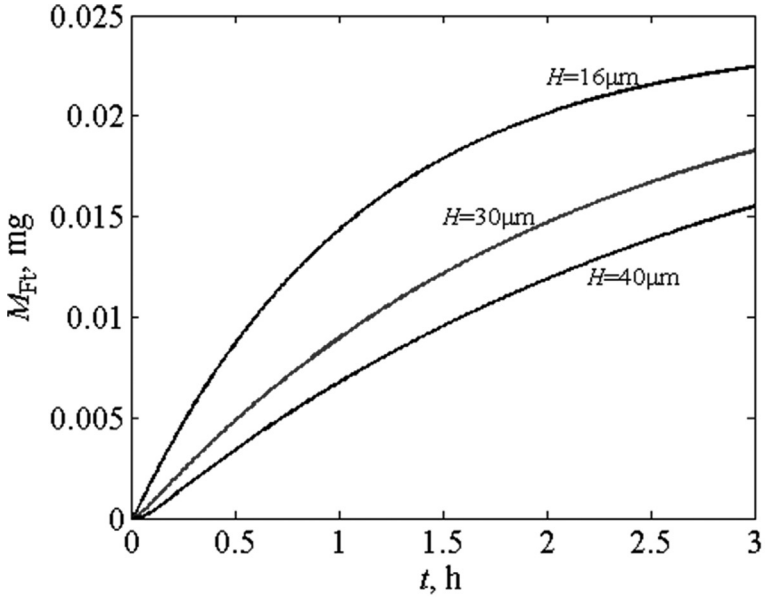

Figure 9. *Transfer kinetics of contaminant into food for various thickness of plastic coating, (L = 48 μm, A = 1 cm², C_{P0} = 5 mg·cm⁻³, k_{CP} = 0.2).*

2. When the initial concentration of contaminant in paper, the value of k_{CP} and the thickness of paper are constant, the amount of contaminant in the food decrease with the increase in thickness of plastic coating, as shown in Figure 8 and Figure 9. Correspondingly, the residue of the contaminant in plastic coating increases, which translates into more protection to the food against contamination a thickness of plastic coating increases.

3.2. Polymer-polymer Bi-layer Packaging System

The bi-layer polymer-polymer packaging system is made up one layer with a contaminant such as recycled polymer and one virgin layer (functional barrier) of the same polymer material. Therefore, the diffusivities in the two layers are identical and the partition coefficient k_{CP} at the interface of the recycled polymer and functional barrier is 1. The results for the polymer-polymer bi-layer system are expressed in two ways: (1) the profiles of contaminant concentration developed through the packaging; and (2) the transfer kinetics of contaminant into functional barrier and food. For this system, Equations (9), (10), (12), and (13) are simplified to obtain Equations (14), (15), (16), and (17), respectively.

$$C'_C = 2C_{P0}\sum_{n=1}^{\infty}\frac{\sin^2\beta_n L\cos\beta_n H\sin\beta_n(H-x)}{\beta_n(L\cos^2\beta_n H + H\sin^2\beta_n L)}e^{-D'\beta_n^2 t} \quad (14)$$

$$C'_P = 2C_{P0}\sum_{n=1}^{\infty}\frac{\sin\beta_n L\cos^2\beta_n H\cos\beta_n(x+L)}{\beta_n(L\cos^2\beta_n H + H\sin^2 L\beta_n)}e^{-D'\beta_n^2 t} \quad (15)$$

$$M'_{Ct} = 2C_{P0}\sum_{n=1}^{\infty}\frac{(1-\cos\beta_n H)\sin^2\beta_n L\cos\beta_n H}{\beta_n^2(L\cos^2\beta_n H + H\sin^2\beta_n L)}e^{-D'\beta_n^2 t} \quad (16)$$

$$M'_{Ft} = -\frac{2AC_{P0}}{\beta_n^2}\sum_{n=1}^{\infty}\frac{\sin^2\beta_n L\cos\beta_n H}{L\cos^2\beta_n H + H\sin^2\beta_n L}(e^{-D'\beta_n^2 t}-1) \quad (17)$$

β_n (n = 1, 2, 3, . . .) is positive root of Equation (18)

$$\cot\beta L = \tan\beta H \quad (18)$$

where C'_C and C'_P are the concentration of contaminant in virgin polymer and recycled polymer, respectively. M'_{Ct} and M'_{Ft} are the amounts of concentration in virgin polymer and food.

The diffusivities in the two layers were assumed to be 10^{-8} according to previous studies in order to make the analysis convenient. The concentration of contaminant is initially uniform in the recycled polymer and zero in the virgin polymer. The results are expressed in two ways: (1) the profiles of contaminant concentration through the packaging, and (2) the transfer kinetics of contaminant into the functional barrier and food. The trends observed in this study are consistent with those observed in other studies (Laoubi *et al.* [13], Feigenbaum *et al.* [15], Rosca *et al.* [16]).

3.2.1. Profiles of Concentration of Contaminant Developed through the Packaging

The concentration profiles drawn using Equation (14) and (15) are shown in Figure 10 to Figure 13 for various values of thickness ratio $L\cdot(L + H)^{-1}$ ranging from 0.33 to 0.83 with constant total thickness of recycled layer and functional barrier layer. These curves give rise to the following noteworthy features:

1. At the very beginning, the concentration of contaminant fall abruptly at the interface of the two polymer layers down to $C_{P0}/2$ as shown in Figure 10 to Figure 13.

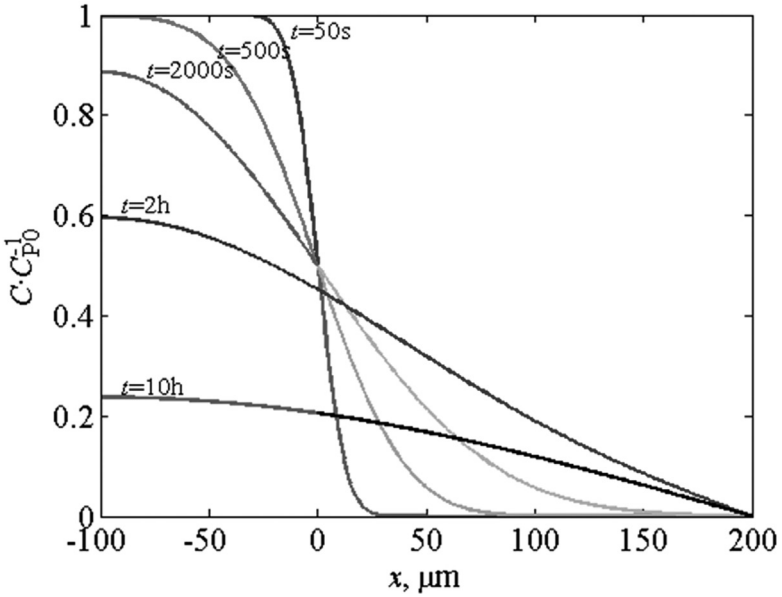

Figure 10. *Profiles of contaminant concentration developed through polymer-polymer bi-layer packaging with thickness of 300 μm for various values of time, $(L\cdot(L + H)^{-1} = 0.33$, $L = 100$ μm, $H = 200$ μm).*

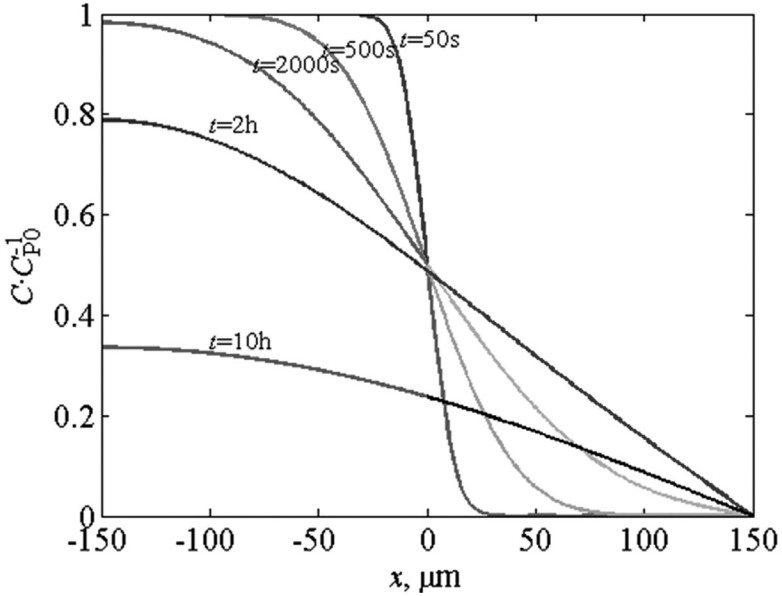

Figure 11. *Profiles of contaminant concentration developed through polymer-polymer bi-layer packaging with thickness of 300 μm for various values of time, $(L\cdot(L + H)^{-1} = 0.5$, $L = 150$ μm, $H = 150$ μm).*

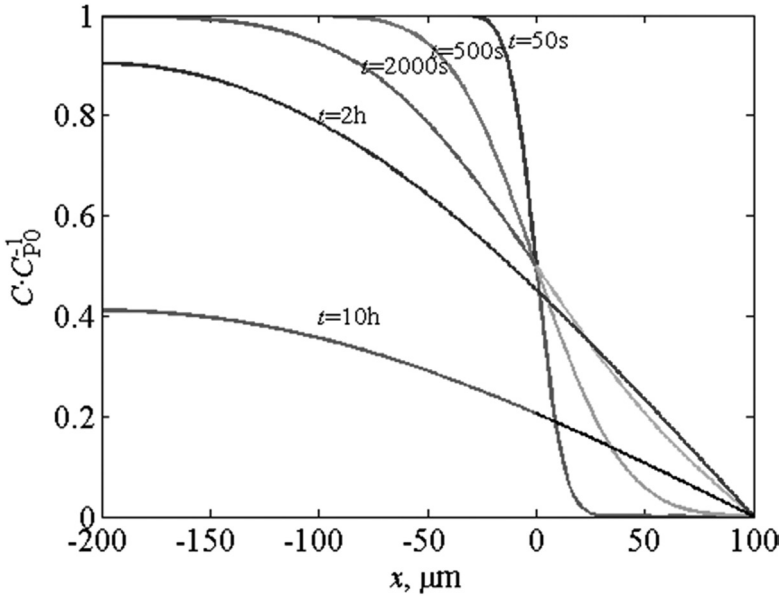

Figure 12. *Profiles of contaminant concentration developed through polymer-polymer bi-layer packaging with thickness of 300 μm for various values of time, $(L \cdot (L + H)^{-1} = 0.67$, $L = 200$ μm, $H = 100$ μm).*

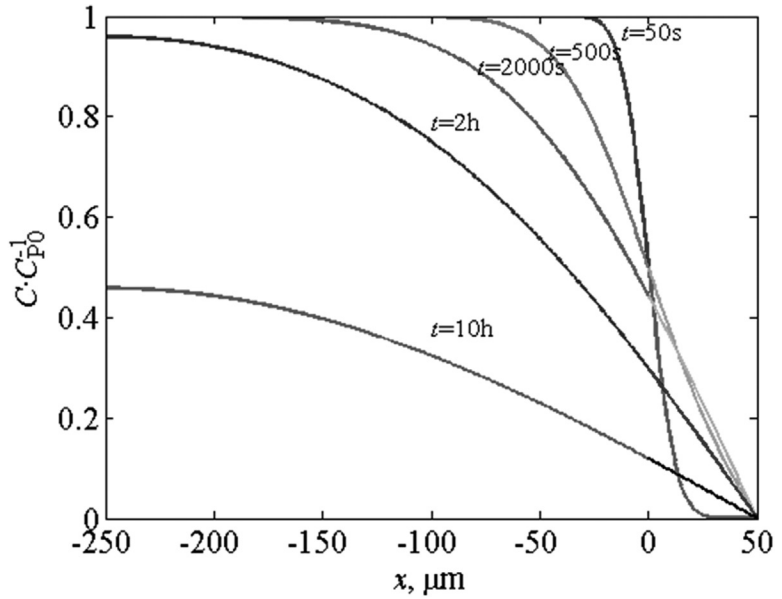

Figure 13. *Profiles of contaminant concentration developed through polymer-polymer bi-layer packaging with thickness of 300 μm for various values of time, $(L \cdot (L + H)^{-1} = 0.83$, $L = 50$ μm, $H = 250$ μm).*

2. At the very beginning, the profiles in the two layers are symmetrical with the point of symmetry at the interface where $C/C_{P0} = 1/2$, regardless of the thickness of layers as shown in Figure 10 to Figure 13.
3. The decreasing rate of contaminant concentration becomes slower with time. The gradient of the concentration is flat on the external surface of recycled layer, namely $x = -L$. At $x = H$ the contaminant concentration is zero.

3.2.2. Kinetics of Transfer of Contaminant into the Functional Barrier and Food

The kinetics equations for contaminant transfer from the recycled layer into the functional barrier and food are expressed using Equations (16) and (17). The kinetics curves are drawn for various values of $L\cdot(L + H)^{-1}$ and are shown in Figure 14 and Figure 15. The following conclusions can be drawn from the curves.

1. A vertical tangent and steep slope are observed at the beginning of the process as shown in Figure 14 and Figure 15. The steep slope shown in Figure 14 results from the perfect contact between the two polymer layers at $x = 0$.

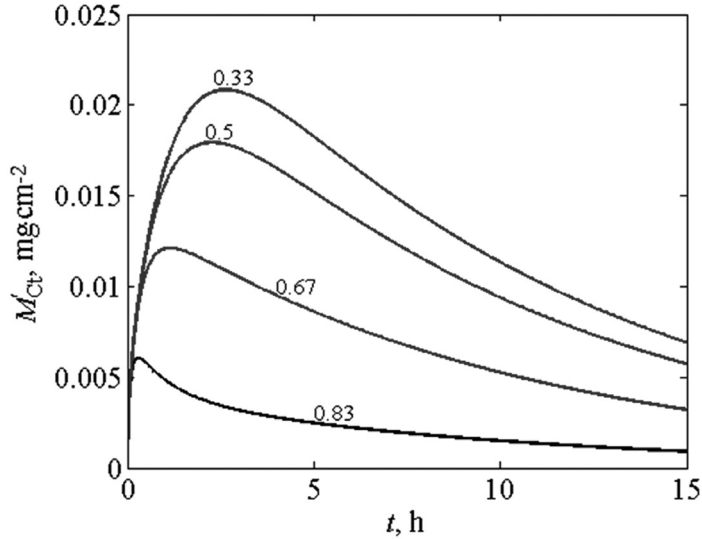

Figure 14. *Transfer kinetics of contaminant in functional barrier for different values of $L\cdot(L + H)^{-1}$, ($(L + H) = 300$ μm, $C_{P0} = 5$ mg·cm^{-3}).*

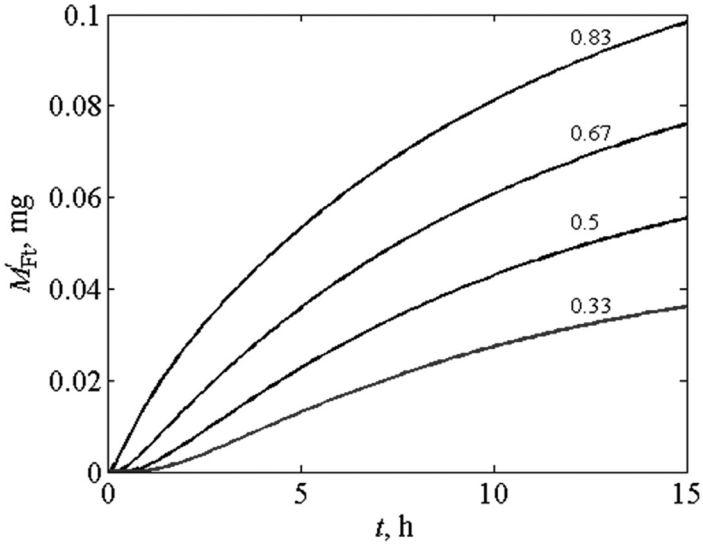

Figure 15. *Transfer kinetics of contaminant in food for different values of $L\cdot(L + H)^{-1}$), ((L + H) = 300 μm, A = 1 cm^2, C_{P0} = 5 mg·cm^{-3}).*

2. The rate of mass transfer decreases with time as shown in Figure 14 and Figure 15.
3. Initially, the virgin polymer layer plays the role of functional barrier as shown in Figure 15.

The amount of contaminant in food is zero. This corresponds to a lag time behavior. The virgin layer shows a high efficiency with the increase of its thickness, that is, the decrease of the ratio of $L\cdot(H + L)^{-1}$. At the same time, the amount of the contaminant entering the food decreases as shown in Figure 15, and most contaminants stay in the virgin polymer layer as shown in Figure 14. The functional barrier delays the migration of contaminant into food, especially with thicker layers of the functional barrier.

4. CONCLUSIONS

For food packaging system such as paper-plastic coating layer-food, the problem of transfer of contaminant from paper through plastic coating into food is complex. As shown in this analysis, different diffusivities in two layers materials and distribution of contaminant between two layers should be considered accordingly. Analytical solutions taking the

facts into account are obtained for the case of a *Fickian* diffusion through the packaging with different diffusivities in paper and plastic coating and partition coefficient at the interface of paper and plastic coating.

The theoretical results are expressed from two aspects: (1) paper-plastic coating layer food packaging system; (2) the applicability of model for bi-layer polymer packaging. Transfer kinetics of contaminant into plastic coating and food, and profiles of concentration of contaminant through the packaging for various values of k_{CP}, and kinetics of transfer of contaminant into plastic coating and food for various thickness of paper and plastic coating are studied for packaging system (1). Profiles of the concentration of contaminant developed through the packaging, and kinetics of transfer of contaminant into functional barrier and food are studied for bi-layer polymer packaging, namely for packaging system (2). According to the curves trend and simplifying of equations, the conclusion can be obtained: the model is of using universality, not only using paper-plastic coating packaging but using bi-layer plastic packaging.

5. NOMENCLATURE

C_P concentration of contaminant in paper, mg·cm^{-3}
D_P diffusion coefficient of contaminant in paper, cm^2·s^{-1}
C_C concentration of contaminant in plastic coating, mg·cm^{-3}
D_C diffusion coefficient of contaminant in plastic coating, cm^2·s^{-1}
k_{CP} partition coefficient of contaminant between plastic coating and paper
C_{P0} initial concentration of contaminant in paper, mg·cm^{-3}
C_{in} initial concentration of contaminant in recycled film, mg·cm^{-3}
M_{Ct} amount of concentration in plastic coating, mg·cm^{-2}
M_{Ft}, M'_{Ft} amount of concentration in food, mg
L thickness of paper, cm
H thickness of plastic coating, cm
R thickness of recycled film, cm
L_F thickness of virgin film, cm
C'_C concentration of contaminant in virgin polymer, mg·cm^{-3}
C'_P concentration of contaminant in recycled polymer, mg·cm^{-3}
M'_{Ct} amount of concentration in virgin polymer, mg·cm^{-2}

6. ACKNOWLEDGMENTS

The authors acknowledge the support of this research by the Opening Fund of Key Laboratory of Product Packaging and Logistics of Guangdong Higher Education Institutes at Jinan University(D.10-0109-11-014), Shanghai Committee of Science and Technology(12dz1125702), as well as Shanghai Young College Teacher' Training-funded Projects(B.37-0109-11-003). Jun Wang and Xiuling Huang contribute equally to this paper as co-first authors.

REFERENCES

1. M.J. Hagenbarth. Paper and paperboard industry protocol for sampling and analysis of recycled materials intended for food packaging applications. *Food Addit. Contam.,* 22(10), 1042–1052 (2005).
2. T. Richter, T. Gude, T. Simat. Migration of novel offset printing inks from cardboard packaging into food. *Food Additives and Contaminants,* 26(12): 1574–1580 (2009).
3. A. Sanches-Silva, S. Pastorelli, J.M. Cruz, C. Simoneau, I. Castanheira, P. Paseiro-Losada. Development of a method to study the migration of six photoinitiators into powdered milk. *J. Agric. Food Chem.,* 56(8): 2722–2726 (2008).
4. R. Koivikko, S. Pastorelli, et al. Rapid multi-analyte quantification of benzophenone, 4-methylbenzophenone and related derivatives from paperboard food packaging. *Food Additives and Contaminants,* 27(10): 1478–1486 (2010).
5. A. Ozaki, T. Ooshima, Y. Mori. Migration of dehydroabietic and abietic acids from paper and paperboard food packaging into food-simulating solvents and Tenax TA., *Food Additives and Contaminants,* 23(8): 854–860 (2006).
6. A. Sturaro, R. Rella, G. Parvoll, D. Ferrara, F. Tisato. Contamination of dry foods with trimethyldiphenylmethanes by migration from recycled paper and board packaging. *Food Additives and Contaminants,* 23(4): 431–436 (2006).
7. Q.B. Lin, T.J. Wang, H. Song, B. Li. Analysis of isothiazolinone biocides in paper for food packaging by ultra-high-performance liquid chromatography-tandem mass spectrometry. *Food Additives and Contaminants,* 27(12): 1775–1781 (2010).
8. G.V. Pace, T.G. Hartman. Miration studied of 3-chloro-1,2-propanediol (3-MCPD) in polyethylene extrusion-coated paperboard food packaging. *Food Addit. Contam.,* 27(6), 884–891 (2010).
9. S.M. Johns, S.M. Jickells, W.A. Read, L. Castle. Studies on functional barriers to migration. 3.migration of benzophenone and model ink components from cartonboard to food during frozen storage and microwave heating. *Packag. Technol. Sci.,* 13(3), 99–104 (2000).
10. Y.S. Song, T. Begley, K. Paquette, V. Komolprasert. Effectiveness of polypropylene film as a barrier to migration from recycled paperboard packaging to fatty and high-moisture food. *Food Addit. Contam.,* 20(9), 875–883 (2003).
11. J. K. Choi, F. Jitsunari, F. Asakawa, H. J. Park, D. S. Lee. Migration of surrogate contaminants in paper and paperboard into water through polyethylene coating layer. *Food Addit. Contam.,* 19(12), 1200–1206 (2002).
12. S. Laoubi, J. M. Vergnaud. Process of contaminant transfer through a food packaging made of a recycled film and a functional barrier. *Packag. Technol. Sci.,* 8(2), 97–110 (1995).
13. S. Laoubi, J. M. Vergnaud. Modelling transport between a monolayer and a bi-layer polymeric package and food. *Food Addit. Contam.,* 14(6–7), 641–647 (1997).
14. O. Piringer, R. Franz, M. Huber, T. H. Begley, T. P. McNeal. Migration from food packaging

containing a functional barrier: mathematical and experimental evaluation. *J. Agric. Food Chem.,* 46(4), 1532–1538 (1998).

15. A. Feigenbaum, S. Laoubi, J. M. Vergnaud. Kinetics of diffusion of a pollutant from a recycled polymer through a functional barrier: recycling plastics for food packaging. *J. Appl. Polym. Sci,* 66(3): 597–607 (1998).
16. I. D. Rosca, J. M. Vergnaud. Transfer of contaminant into solid food from a bottle made of bilayer polymer with a recycled and virgin layer: effect of the thickness of these polymer layers. *J. Appl. Polym. Sci.,* 66(7), 1291–1301 (1998).
17. P. Y. Pennarun, Y. Ngono, P. Gole, A. Feigenbaum. Functional barriers in PET recycled bottles. Part I: diffusion pollutants during processing. *Applied Polymer Science,* 92, 2859–2870 (2004).
18. P. Dole, Y. Voulzatis, O. Vitrac, A. Reynier, T. Hankemeier, S. Aucejo, A. Feigenbaum. Modelling of migration from multi-layers and functional barriers: estimation of parameters. *Food Addit. Contam.,* 23(10), 1038–1052 (2006).
19. J. Crank. *The mathematics of diffusion* (2nd ed.), Oxford: Clarendon Press, (1975).
20. H. S. Carslaw, J. C. Jaeger. *Conduction of heat in solids* (2nd ed.), Oxford University Press, (1959).
21. T. Begley, L. Castle, A. Feigenbaum, R.Franz. Evaluation of migration models that might be used in support of regulations for food-contact plastics. *Food Addit. Contam.,* 22(1), 73–90 (2005).

Equivalent Drop Test for Structural Pulp Mould Cushion

CHEN ZHONG[1] and KATSUHIKO SAITO[2,*]

[1]*Ph.D. Candidate, Kobe University, Fukaeminami, Higashinada, Kobe, Japan*

[2]*Professor, Ph.D. in Engineering, Transport Packaging Laboratory, Kobe University, Fukaeminami, Higashinada, Kobe, Japan*

ABSTRACT: To address the limitations of the conventional equivalent drop theory, we proposed a friction equivalent drop theory in previous studies. However, our proposal was speculative and a complete proof was not attained. To substantiate the robustness of this new theory, further investigation has been undertaken. A structural pulp mould cushion is used as the test material. A chi-square fit test is used to examine the corrective effect of the friction equivalent drop theory qualitatively. We also evaluate the corrective effect quantitatively using a correction indicator. The results show that the friction equivalent drop theory can be applied to a structural pulp mould cushion. The corrective effects are not constant under varied stress but become more prominent as the lowest point of the cushion curve is approached.

INTRODUCTION

A transport package is necessary to ensure the safe delivery of products from manufacturers to consumers. According to JIS Z 0240 (2002) [1] (this standard corresponds with ISO 8568 (1989) [2], the majority of transport packages are constructed from structural cushioning material (SCM) (For example, a corrugated box and pulp mould cushions in Figure 3 are SCM.). To verify whether an optimal transport package is designed, an equivalent drop test or a dynamic compression test is often performed [3].

Generally, the conventional equivalent drop theory (conventional theory) is applied [3,4]. Theoretically, the dynamic compression and equivalent drop tests yield the same results for equal drop heights. However, Saito *et al.* [5,6] proved that the conventional theory has limitations that result in errors; dynamic compression test results differ from equivalent drop test results even when the drop heights are the

*Author to whom correspondence should be addressed. E-mail: ksaito@maritime.kobe-u.ac.jp

1557-7244/12/03 185-17

Figure 1. *Schematic diagram of friction-viscous damping (FVD) model. (a) Product and SCM unit; (b) FVD model.*

same. Zhong *et al.* developed a friction equivalent drop theory (friction theory) [7] by assuming a product and SCM unit as a friction-viscous damping (FVD) model (Figure 1) [8,9]. Using the friction theory, the peak response acceleration (PRA) of the dynamic compression test, $A_{ff\,\max}$, and the equivalent drop test, $A_{cs\,\max}$, are expressed by Equations (1) and (2), respectively, and a correction condition is given by Equation (3).

$$A_{ff\ \max} = u_{ff} \cdot \omega_n \cdot V + \mu_{ff} \cdot \omega_n \cdot V_F \tag{1}$$

$$A_{cs\ \max} = u_{cs} \cdot \omega_n \cdot V_c \tag{2}$$

$$V_{\text{new}} = \frac{u_{cs}}{u_{ff}} V_c - \frac{\mu_{ff}}{u_{ff}} V_F \tag{3}$$

where ω_n is the natural angular frequency, u_{ff}, u_{cs} and μ_{ff} are correcting coefficients, V is the impact velocity of the mass, V_c is the velocity change of the equivalent drop test, V_{new} is the corrected impact velocity and V_F is the velocity related to friction.

Using the correction condition of the friction theory, we can correct the equivalent accuracy of the dynamic compression test. The correction process is shown in Figure 2 [7].

- *Step 1:* simulations are conducted to calculate u_{ff} and μ_{ff};
- *Step 2:* the friction F_c is deduced to calculate V_F;
- *Step 3:* using the equivalent drop test data on the basis of the conventional theory, u_{cs} is calculated.
- Finally, V_{new} is calculated by Equation (3).

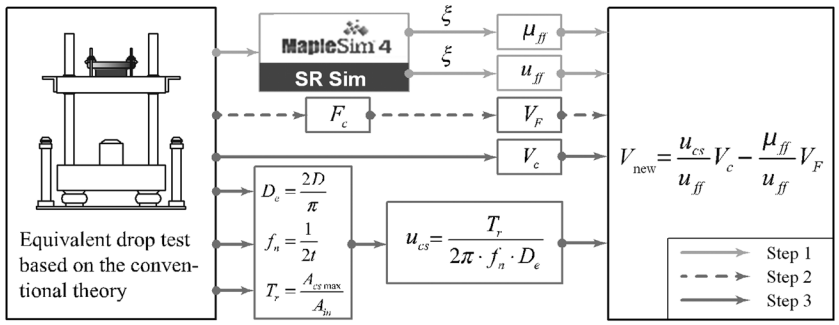

Figure 2. *Schematic diagram of how to correct the equivalent accuracy of the dynamic compression test using the friction theory.*

Zhong *et al.* [7] showed that the application of the friction theory can improve the equivalent precision of SCM tests. However, this conclusion was not fully verified. To obtain a robust conclusion, it is necessary to consider other factors, such as stress, test material or free fall height. In this study, we addressed the stress factor. For many applications, a pulp mould cushion is often considered as a sustainable packaging material; it is produced from recycled materials and can be recycled again after its useful life-cycle [10]. Pulp mould cushions, illustrated in Figure 3(a), are widely used in transport packaging. To study the friction theory, we simplified an actual pulp mould cushion, shown in Figure 3(b). We used the simplified pulp mould cushion unit to explore a corrective effect using the friction theory under various stress conditions.

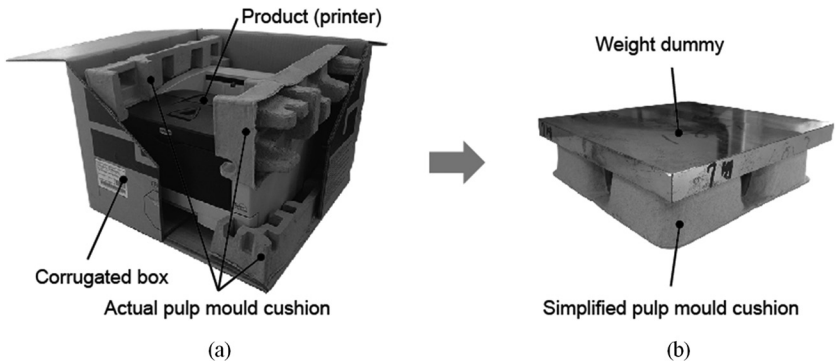

Figure 3. *Pulp mould cushions. (a) Actual pulp mould cushion package; (b) Simplified pulp mould cushion unit.*

EQUIPMENT AND MATERIALS

Test Equipment

We used a dynamic compression tester to perform the dynamic compression tests and a shock machine to perform the equivalent drop tests. An acceleration analysis instrument known as the 'Shock manager', was used to measure the response acceleration in the two tests. All test equipment was made by Yoshida Seiki Co., Ltd., Japan.

Weight Dummy

Nine weight dummies, ranging between 4 and 12 kg in one kilogram increments, were used [Figure 3(b)]. The length and width (220 × 220 mm) of the dummies were constant but the thickness varied.

Pulp Mould

Based on previous studies [7–9], and taking the technical specifications of the test equipment into consideration [11,12], we used the simplified pulp mould (208 × 208 mm) illustrated in Figure 4(a). To obtain a good response acceleration curve, the appropriate height of the pulp mould was determined to be 50 mm. The 'Slush moulding' process was applied to this pulp mould. The walls of the pulp mould were 3 mm thick; the surface of inside was very rough and the other was moderately smooth. Figure 4(a) illustrates the three dimensional structure of the pulp mould. A cross-section view of the pulp mould is shown in Figure 4(b).

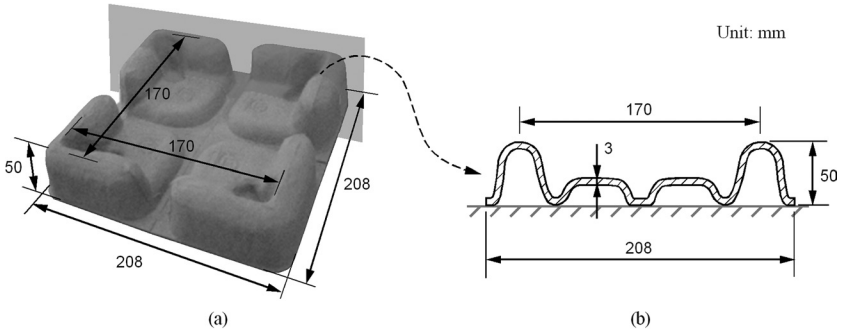

Figure 4. *Test material. (a) Three dimensional structure of pulp mould; (b) Cross-section view of pulp mould.*

DATA COLLECTION AND TEST DESIGN

Data Collection

According to JIS Z 0240 (2002), 0.6 m represents the general drop height during the transportation. Therefore, the drop height, H, was set to 0.6 m and was constant for all experiments. We obtained the theoretical impact velocity of the mass V_{th} = 3.43 m/s using the equation $V_{th} = \sqrt{2gH}$. According to the conventional theory, $V_c = V_{th} = 3.43$ m/s.

In earlier studies [6,8,13], data were used only when V or V_c = 3.43 m/s for both tests. In this study, to improve the accuracy of the test results, we redefined the effective impact velocity, V, and the effective velocity change, V_c, to a range of 3.43 ± 0.10 m/s. All data in the range of 3.43 ± 0.10 m/s were recorded.

Test Design

The flow of the test is illustrated in Figure 5. The test was broadly divided into data acquisition and data analysis.

During the data acquisition stage, the experiment was repeated using nine 4–12 kg dummies. The test method was as follows:

- *Step i:* We performed the equivalent drop test and recorded V_c and $A_{cs\ max}$.
- *Step ii:* Based on the conventional theory and using the impact pulse of the equivalent drop test in Step i, we carried out the dynamic compression test and recorded V and $A_{ff\ max}$.
- *Step iii:* Following the correction method, as shown in Figure 2, we corrected V using the data recorded in Steps i and ii. In certain cases, the resulting V_{new} was not in the 3.43 ± 0.10 m/s range.
- *Step iv:* If V_{new} was not within 3.43 ± 0.10 m/s, the dynamic compression test was re-performed to measure the new PRA corresponding to the V_{new}.

In the data analysis stage, we processed all of experimental data collected in the data acquisition stage. We examined the corrective effect of the friction theory on the pulp mould.

To ensure the reliability of the results [14], we collected 30 sets of data for each of the three tests (Steps i, ii and iv). We used nine weight dummies. Therefore, 30 × 3 × 9 = 810 experiments were necessary.

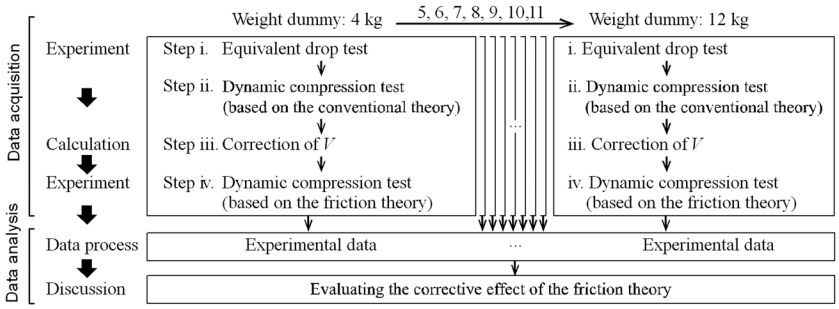

Figure 5. *Test flow.*

TEST RESULTS

Acceleration–Time Curve

The acceleration–time curve of SCM such as a sleeve was an unsmooth curve that is similar to saw tooth, according to the previous study [8]. However, the acceleration–time curve of the pulp mould (the equivalent drop test using the 10 kg dummy), shown in Figure 6, is very smooth.

Figure 7 shows a schematic diagram of the relative position of the weight dummy and the pulp mould before and after the equivalent drop test. By analysing the state of the pulp mould before and after compression, it is evident that there is a line contact (There is a line contact in three dimensional space although it is shown as an immediate point

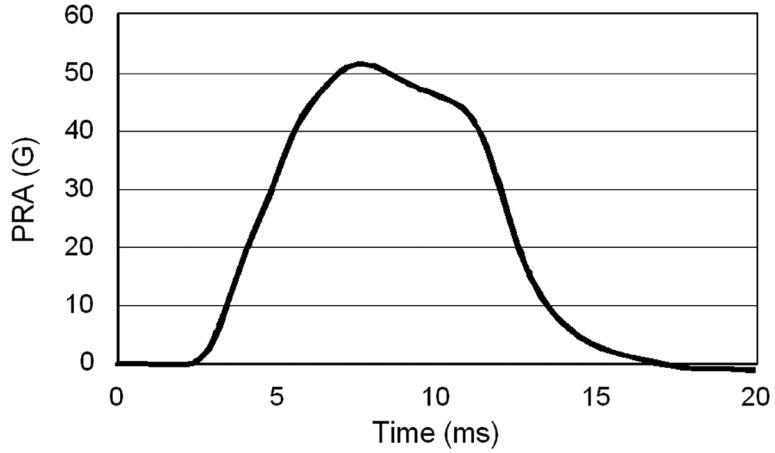

Figure 6. *Acceleration–time curve of pulp mould. Equivalent drop test using a 10 kg dummy.*

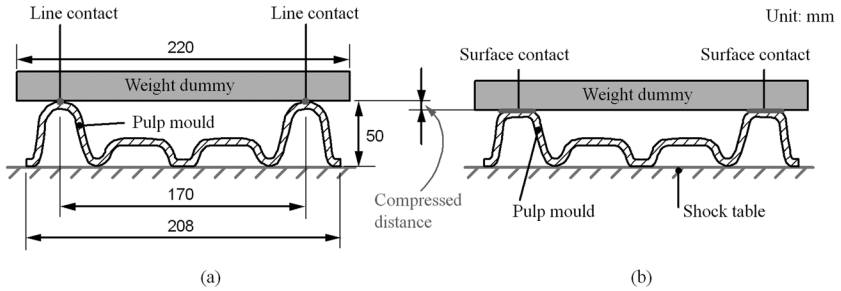

Figure 7. *Schematic diagram of compression process of the pulp mould. (a) Before compression; (b) After compression.*

contact in Figure 7(a)) between the pulp mould and the weight dummy at initial impact. However, the line contact gradually becomes a surface contact when the impact happens. The gradual deformation results in a smooth acceleration–time curve.

Probability Distribution of the Difference in the PRA of the Two Tests

The difference in the PRA of the two tests (dGs) is an important indicator for this study. dGs is expressed as [15]

$$\mathrm{dGs} = A_{cs\ \max}(V_c) - A_{ff\ \max}(V) \tag{4}$$

For the conventional theory, dGs should be 0 G theoretically. For the friction theory, there is a relationship between dGs and the corrective effect; the bigger the dGs value, the smaller the corrective effect. Thus, if we know dGs, we can determine the approximate corrective effect of the friction theory.

An example of the calculation procedure for dGs values is presented in Table 1. The complete data set is too large to include in the example. Therefore, only a portion of the data is shown. The procedure involves three steps.

1. The test results of the equivalent drop and dynamic compression tests are listed in order of V_c or V.
2. Values of $A_{cs\ \max}(V_c)$ and $A_{ff\ \max}(V)$ corresponding to the same value of V_c or V are grouped (blocks with same colour).
3. Using all the data in each group, dGs values are calculated by Equation (4).

Table 1. Example of dGs calculation. Dummy: 6 kg.

Equivalent drop test		Dynamic compression test (Conventional theory)		dGs	
Velocity change V_c (m/s)	$A_{csmax}(V_c)$ (G)	Impact velocity V (m/s)	$A_{ffmax}(V)$ (G)	Impact velocity (m/s)	$A_{csmax}(V_c)-A_{ffmax}(V)$ (G)
3.39	80.6	3.39	73.3	3.39	7.3
3.40	79.1	3.39	73.8	3.39	6.8
3.40	80.1	3.40	73.9	3.40	5.2
3.40	80.6	3.41	72.8	3.40	6.2
3.41	77.4	3.41	73.1	3.40	6.7
3.41	79.5	3.42	72.9	3.41	4.6
3.42	82.2	3.42	73.0	3.41	6.7
3.43	79.9	3.43	76.8	3.41	4.3
3.43	80.0	3.43	76.9	3.41	6.4
3.43	80.4	3.43	77.6	3.42	9.3
3.44	81.2	3.43	78.1	3.42	9.2
3.44	81.8	3.44	78.4	3.43	3.1

To plot the probability distribution of dGs, the following data process was conducted.

1. After all dGs values were calculated, the total number of dGs values, N, were counted.
2. The values of dGs were separated by 1 G increments. For example: if dGs ranged between 0 G and 3.4 G, we separated dGs into four parts: $0 \le dGs < 1$, $1 \le dGs < 2$, $2 \le dGs < 3$ and $3 \le dGs < 4$ (G).
3. The number of each dGs parts, n, was counted.
4. The probability, $P = n/N$, was calculated.

The probability distributions of dGs before and after the correction were plotted, as shown in Figure 8. According to statistical theory [14], the probability distribution of dGs after the correction should get even closer to 0 G than before the correction if the friction theory can be applied to SCM when stress varies. By comparing the nine bar charts presented in Figure 8, the following conclusions are drawn. (1) When a light weight dummy is used, dGs is large before and after the correction. (2) dGs reduces gradually relative to the increase in the weight of the dummy. (3) dGs with the highest probability after the correction is closer to 0 G than before the correction. This behaviour is more prominent as the weight dummy becomes heavier.

It should be noted that the bar numbers (x-axis) for aggregated data are not the same among weight dummies due to the varied deviations under different dummies.

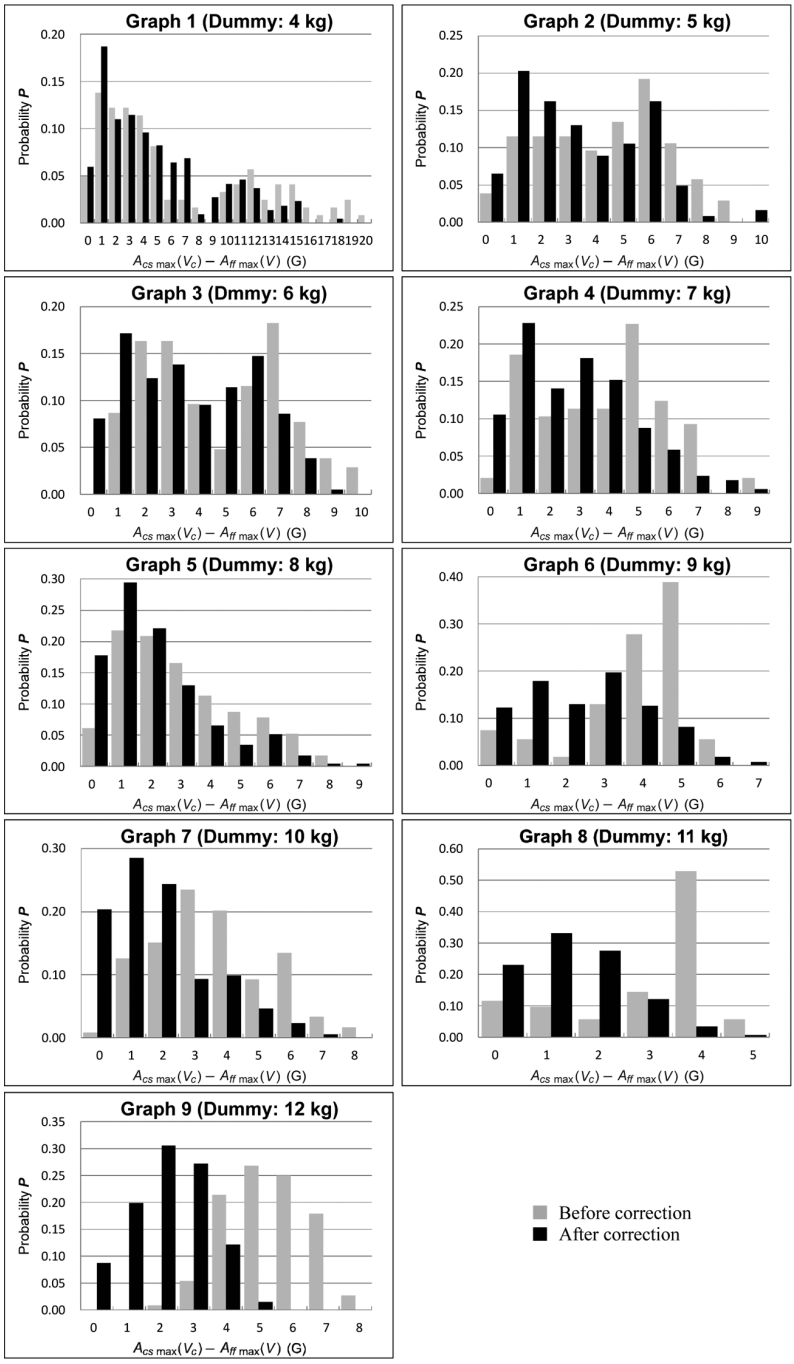

Figure 8. *Probability distributions of dGs among nine weight dummies.*

Chi-square Test [16]

A chi-square test is widely used to compare the distribution of a single variable to an expected distribution. Pearson's chi-squared test (χ^2) is the best-known of several chi-square tests. Pearson's chi-squared test is used to assess goodness of fit, homogeneity and independence. A goodness of fit test establishes whether or not an observed frequency distribution differs from a theoretical distribution. A homogeneity test compares the distribution of counts for two or more groups on the same categorical variable. An independence test assesses whether paired observations on two variables, expressed in a contingency table, are independent. To examine the corrective effect of the friction theory qualitatively, the homogeneity test was used in this study.

The calculation method for the chi-square homogeneity test is as follows:

1. State hypotheses (H_0 and H_a).
2. Find expected values for each cell (V_{exp}).
3. Derive chi-squared statistic (χ^2) using Equation (5). (V_{obs}: the observed value)

$$\chi^2 = \sum_{\text{all cells}} \frac{(V_{obs} - V_{exp})^2}{V_{exp}} \tag{5}$$

4. Determine the critical value of χ^2 (χ^{2*}) using the χ-table based on the degree of freedom (d_f) and the α level.
5. Decision: reject H_0 if $\chi^2 > \chi^{2*}$; accept if otherwise.

Table 2 uses the data from graph 6 in Figure 8 to explain the calculation process for the chi-square homogeneity test. The observed values are shown in left side of Table 2. Based on the experimental data, dGs changes in a range of 0–8 G. Therefore, the column 'dGs' is separated into eight rows. The 'Before correction' and 'After correction' values are the counts of dGs.

There are five steps in the calculation process:

1. Determine the hypotheses. There are two variables: distribution of dGs and application of the friction theory (before and after correction). Therefore, the hypotheses were defined as
   H_0: the distribution of dGs is the same before and after correction;
   H_a: the distribution of dGs is different before and after correction.

Table 2. Observed and Expected Values used in an Example of Chi-square Test.

dGs (G)	Observed Value (V_{obs})			Expected Value (V_{exp})	
	Before Correction	After Correction	Total	Before Correction	After Correction
$0 \le dGs < 1$	4	33	**37**	7	30
$1 \le dGs < 2$	3	48	**51**	10	41
$2 \le dGs < 3$	1	35	**36**	7	29
$3 \le dGs < 4$	7	53	**60**	11	49
$4 \le dGs < 5$	15	34	**49**	9	40
$5 \le dGs < 6$	21	22	**43**	8	35
$6 \le dGs < 7$	3	5	**8**	2	6
$7 \le dGs < 8$	0	2	**2**	0	2
Total	**54**	**232**	**286**		
Observed Distribution	**19%**	**81%**	**100%**		

2. Compute the expected values before and after correction counts by multiplying the overall before and after correction proportions with the total for each category. For example, $0 \le dGs < 1$ (before correction) = 19% × 37 ≈ 7; $4 \le dGs < 5$ (after correction) = 81% × 49 ≈ 40. The expected values are shown in right side of Table 2.
3. Substitute the observed and expected values into Equation (5); χ^2 was calculated as 47.0.
4. Computed χ^{2*}. The degree of freedom d_f = (number of rows – 1) × (number of columns – 1) = (8 – 1) × (2 – 1) = 7. Additionally, a 5% α level was used here. From the χ-table based on d_f = 7 and the 5% α level, it is known that $\chi^{2*} = 14.1$.
5. Because χ^2 is greater than χ^{2*}, reject H_0. The distribution of dGs is different between the before and after correction values.

Similarly, we performed chi-square tests for the other eight tests. The results are presented in Table 3. It is evident that $\chi^2 > \chi^{2*}$ when 6–12 kg dummies were used, although $\chi^2 < \chi^{2*}$ when 4 and 5 kg dummies were used. Therefore, it is evident that the distribution of dGs after correction is more significant than before correction.

It should be noted that chi-square tests only proved variations of dGs before and after the correction. They did not indicate whether the correction resulted in positive or negative changes or the degree to which the corrective effects change. Therefore, we cannot quantitatively eval-

Table 3. Results of Chi-square Tests of Homogeneity for Graphs 1–9 in Figure 8.

Dummy Weight (kg)	4	5	6	7	8	9	10	11	12
d_f	20	10	10	9	9	7	8	5	8
χ^{2*}	31.4	18.3	18.3	16.9	18.3	14.1	15.5	11.1	15.5
χ^2	28.3	17.3	31.5	30.6	24.5	47.0	68.3	162.6	225.0

uate the effects of the friction theory based only on the bar charts of the probability distribution of dGs.

DISCUSSION

As mentioned previously, based on the bar charts of the probability distribution of dGs, we can qualitatively conclude that the friction theory is applicable to SCM under different stresses. However, we cannot evaluate the effects of the application of friction theory quantitatively. Therefore, we address this issue by using a correction indicator. The correction indicator Δ is defined as [15].

$$\Delta = \frac{\Gamma_{\text{before}} - \Gamma_{\text{after}}}{\Gamma_{\text{before}}} \times 100\% \tag{6}$$

where

$$\Gamma_{\text{before}} = \frac{\overline{\Sigma_n (A_{cs\ \max}(V_c) - A_{ff\ \max}(V_{\text{old}}))}}{\overline{A_{ff\ \max}(V_{=3.43})}}$$

$$\Gamma_{\text{after}} = \frac{\overline{\Sigma_n (A_{cs\ \max}(V_c) - A_{ff\ \max}(V_{\text{new}}))}}{\overline{A_{ff\ \max}(V_{=3.43})}}$$

$A_{ff\ \max}(V_{=3.43})$ denotes the true value of the PRA. $A_{ff\ \max}(V_{\text{old}})$ and $A_{ff\ \max}(V_{\text{new}})$ denote the PRA of the dynamic compression test before and after correction, respectively. $A_{\text{cs max}}(V_c)$ denotes the PRA of the equivalent drop test.

The results of the analysis are summarized in Table 4. Column ① lists the weights of the dummies used. Column ② contains the average of $A_{ff\ \max}(V_{=3.43})$. Column ③ shows the average of the friction under different stresses. The data in column ④ correspond to the average of dGs. The data presented in column ⑤ are the standard deviations of dGs. Column ⑥ lists the correction indicator Δ.

Table 4. Data Analysis Results for Pulp Mould.

			④ (G)		⑤ (G)		
① (kg)	② (G)	③(N)	before[a]	after[b]	before	after	⑥
4	106.5	104	6.27	4.91	5.46	4.10	21.82%
5	86.1	81	4.38	3.37	2.37	2.36	23.17%
6	78.0	61	4.82	3.66	2.53	2.31	23.97%
7	65.8	46	3.96	2.81	2.18	1.96	29.07%
8	58.2	39	3.04	2.12	2.02	1.78	30.16%
9	52.4	28	3.04	2.48	1.49	1.63	36.88%
10	47.4	23	3.63	1.93	1.80	1.56	46.74%
11	44.5	16	3.04	1.47	1.43	1.05	51.59%
12	38.7	12	5.42	2.26	1.26	1.14	58.27%

① Dummy weights.
② Average of the PRA of the dynamic compression test when V = 3.43 m/s.
③ Friction.
④ Average of dGs.
⑤ Standard deviations of dGs.
⑥ Correction indicator Δ (a larger value indicates better corrective effect).
[a] Before correction using the friction theory.
[b] After correction using the friction theory.

Using the data in column ②, the cushion curve is plotted, as shown in Figure 9. It is known that the PRA of the dynamic compression test decreases as the dummy weight increases. Based on the equivalent drop theory, the same trend holds true for the equivalent drop test. In this study, additional experiments (hollow points in Figure 9) were per-

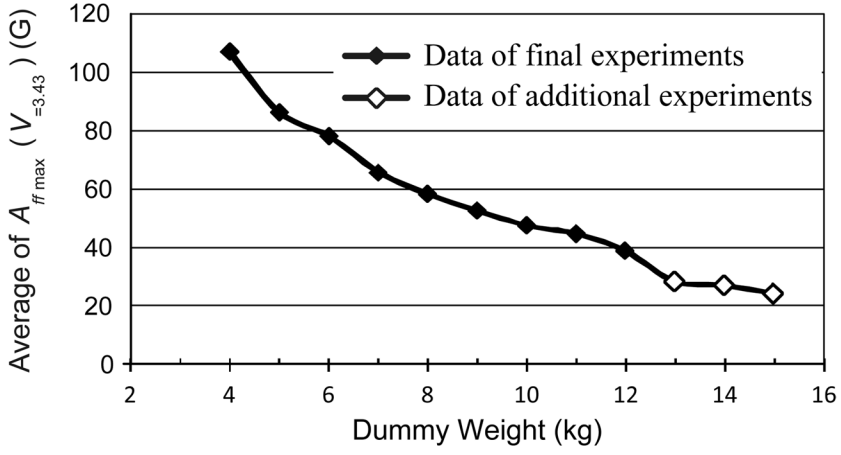

Figure 9. *Cushion curve.*

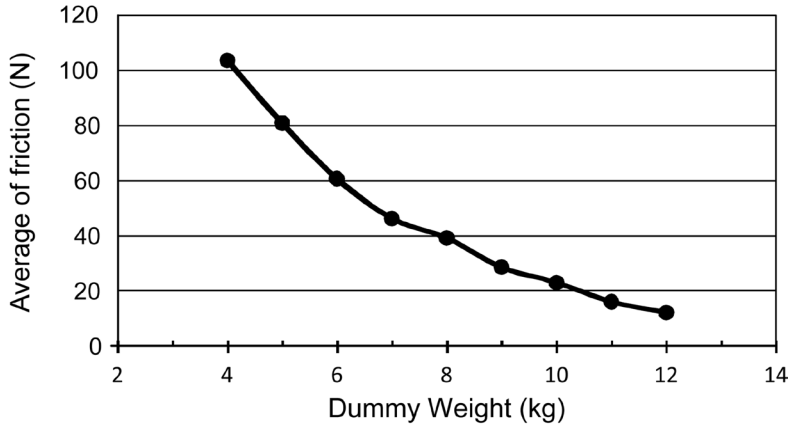

Figure 10. *Friction curve.*

formed to confirm the lowest point of the cushion curve using a 15 kg dummy from which the technical specifications of our test equipment, was the maximum allowable weight [10,11]. However, it was not possible to obtain the lowest point of the cushion curve.

Using the data in column ③, the friction curve is plotted, as shown in Figure 10. Under different stresses, the friction did not remain constant; it decreased as the weight of the dummies increased. In an earlier study [15], the friction, F_c, was expressed as

$$F_c = \frac{1}{4}\frac{E_n}{A} - \frac{\pi}{2}kA \tag{7}$$

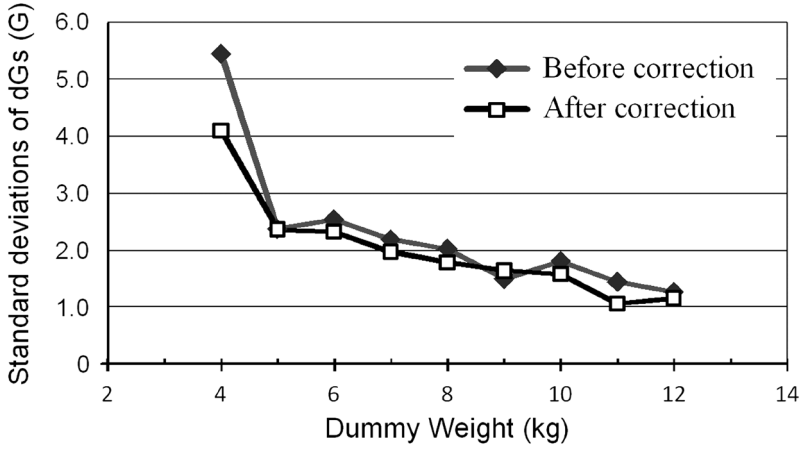

Figure 11. *Standard deviations of dGs curves.*

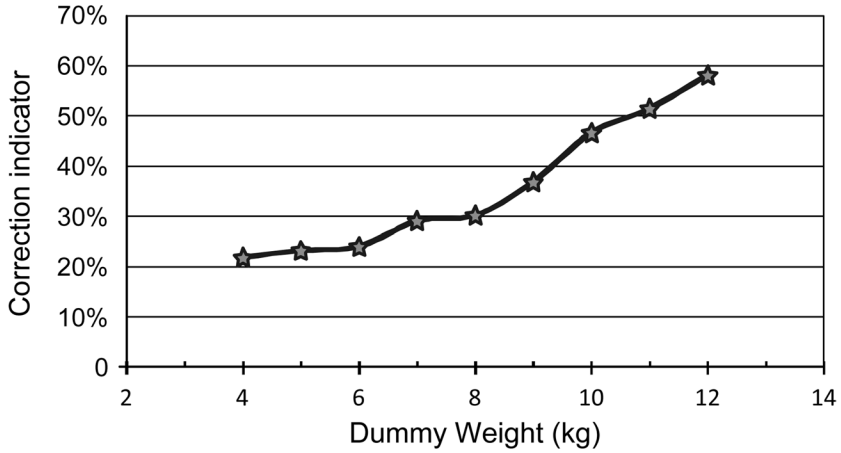

Figure 12. *Correction indicator curve.*

Based on Equation (7), we concluded that if the weight of the dummy increased, F_c will decrease. The friction curve shown in Figure 10 verifies this conclusion.

Using the data in column ⑤, standard deviations of dGs curves among the weight dummies are plotted, as shown in Figure 11. Standard deviations of dGs before and after the correction decrease in respect of the increase of the weight dummy. Standard deviations of dGs after the correction are smaller than those before the correction. The average deviation of dGs has the same behaviour as the standard deviation.

Using the data in column ⑥, the correction indicator curve of the friction theory is plotted, as shown in Figure 12. Here, the correction indicator is denoted by a percentage. This number represents the degree by which the application of the friction theory can improve the equivalent precision of the two tests with respect to the results before the correction. A larger value indicates a better corrective effect. The corrective effects corresponding to the 4–6 kg dummies are approximately 20%, and the corrective effect corresponding to the 12 kg dummy is approximately 60%. It is clear that the corrective effect becomes more significant as the weight of the dummy increases.

CONCLUSIONS AND FURTHER STUDY

To substantiate the robustness of the friction equivalent drop theory proposed in our previous work [7], a follow-up study was performed. In this study, a structural pulp mould cushion was used as the test material,

and dynamic compression and equivalent drop tests were performed. Initially, we investigated the corrective effect of the friction equivalent drop theory qualitatively using probability distributions of dGs among varying weight dummies. The results showed that the friction equivalent drop theory can be applied to a structural pulp mould cushion. We also evaluated the corrective effect quantitatively using a correction indicator. These results showed that the corrective effects are not under constant varied stress but become more prominent as the lowest point of the cushion curve is approached. In a previous study [15], we also explored the influence of stress using a sleeve as the test material. The conclusions of the test using the sleeve were consistent with those reported in this paper.

To clarify the practical significance of this study, the corrective effect of the application of the friction equivalent drop theory for an actual package dummy will be addressed in a future study. Using the actual package dummy, we intend to perform equivalent drop tests to obtain metadata. As well, digital simulations will be run and an evaluation method that can be used to improve the efficiency and accuracy of transport package design will be proposed.

REFERENCES

1. JIS Z 0240. 2002. “Structural Cushioning Materials for Packaging—Determination of Cushioning Performance”.
2. ISO 8568. 1989. “Mechanical shock—Testing machines—Characteristics and performance”.
3. Katsuhiko SAITO and Kiyohide HASEGAWA. 2008. *Foundation and Applications of Transport Package* (in Japanese), Saiwaishobo Inc.
4. Katsuhiko SAITO and Kazuaki KAWAGUCHI, “Equivalent Drop Theory with Damping”, *23rd International Association of Packaging Research Institutes Symposium,* Vol.3, No.5, 2007, pp. 255–260.
5. Kazuaki KAWAGUCHI and Katsuhiko SAITO, “Experimental verification of equivalent drop testing with damping for packaged freight”, *Journal of Packaging Science & Technology,* Japan, Vol.17, No.1, 2008, pp. 39–45.
6. Katsuhiko SAITO and Chen ZHONG, “Modified Simulated Drop Test for Transmitted Shock Characteristics of Structural Plastic Foam Cushioning Materials”, *17th IAPRI World Conference on Packaging,* 2009, pp. 491–495.
7. Chen ZHONG, Katsuhiko SAITO and Kazuaki KAWAGUCHI, “Improvement of Equivalent Drop Theory for Transport Packaging”. *Wiley Online Library (wileyonlinelibrary.com) DOI: 10.1002/pts.1961*. (Oral presentation at 18th IAPRI World Conference on Packaging, and published online on the *Packag. Technol. & Sci.* dedicated 2012 IAPRI Symposium page).
8. Chen ZHONG and Katsuhiko SAITO, “Modified Simulated Drop Test for Transmitted Shock Characteristics of Structural Corrugated Fiberboard”, *Journal of Applied Packaging Research,* Vol. 4, No. 4, 2010, pp. 189–201.
9. Chen ZHONG, Katsuhiko SAITO and Kazuaki KAWAGUCHI, “Shock Response of Frictional-viscous Damping Model for Cushioning Package”, *Journal of Applied Packaging Research,* Vol. 5, No. 4, 2011, pp. 197–214.

10. http://en.wikipedia.org/wiki/Molded_pulp. (Accessed in August 2012)
11. Yoshida Seiki Co., Ltd.. *Shock Machine User's Guide* (in Japanese). ASQ-700 serial.
12. Yoshida Seiki Co., Ltd.. *Dynamic Compression Tester User's Guide* (in Japanese). ACST-200 serial.
13. Chen ZHONG and Katsuhiko SAITO, "Equivalent Drop Test Modification for Determination of Cushioning Performance", *Journal of Packaging Science & Technology,* Japan, Vo. 19, No. 2, pp. 123–135.
14. Robert V. Hogg, Joseph W. McKean and Allen T. Craig. 2005. *Introduction to Mathematical Statistics* (Sixth Edition), Pearson Education.
15. Chen ZHONG and Katsuhiko SAITO, "Modified Equivalent Drop Test for Structural Corrugated Fiberboard Cushioning", *Journal of Packaging Science & Technology,* Japan, Vol. 21, No. 4, 2012, pp. 281–293.
16. Priscilla E. Greenwood and Mikhail S. Nikulin. 1996. *A Guide to Chi-Squared Testing,* Wiley-Interscience.

Guide to Authors

1. Manuscripts shall be sent electronically to the editors, Changfeng Ge at cfgmet@rit.edu and Bruce Welt at bwelt@ufl.edu using Microsoft Word in an IBM/PC format. If electronic submission is not possible, three paper copies of double-spaced manuscripts may be sent to Changfeng Ge, Editor of the *Journal of Applied Packaging Research*, Rochester Institute of Technology, One Memorial Drive, Rochester, NY 14623-5603, USA (Telephone 585-475-5391) or Bruce Welt, Editor of the *Journal of Applied Packaging Research*, University of Florida, Box 110570, Gainesville, FL 32611-0570, USA (Telephone 352-392-1864, X-111). Manuscripts should normally be limited to the space equivalent of 6,000 words. The editor may waive this requirement in special occasions. As a guideline, each page of a double-spaced manuscript contains about 300 words. Include on the title page the names, affiliations, and addresses of all the authors, and identify one author as the corresponding author. Because communication between the editor and the authors will be electronic, the email address of the corresponding author is required. Papers under review, accepted for publication, or published elsewhere in journals are normally not accepted for publication in the *Journal of Applied Packaging Research*. Papers published as proceedings of conferences are welcomed.
2. Article titles should be brief, followed by the author's name(s), affiliation, address, country, and postal code (zip) of author(s). Indicate to whom correspondence and proofs should be sent, including telephone and fax numbers and e-mail address.
3. Include a 100-word abstract and keywords.
4. If electronic art files are not supplied, submit three copies of camera-ready drawings and glossy photographs. Drawings should be uniformly sized, if possible, planned for 50% reduction. Art that is sent electronically should be saved in either a .tif or .JPEG files for superior reproduction. All illustrations of any kind must be numbered and mentioned in the text. Captions for illustrations should all be typed on a separate sheet(s) and should be understandable without reference to the text.
5. DEStech uses a numbered reference system consisting of two elements: a numbered list of all references and (in the text itself) numbers in brackets that correspond to the list. At the end of your article, please supply a numbered list of all references (books, journals, web sites etc.). References on the list should be in the form given below. In the text write the number in brackets corresponding to the reference on the list. Place the number in brackets inside the final period of the sentence cited by the reference. Here is an example [2].

   Journal: 1. Halpin, J. C., "article title", *J. Cellular Plastics,* Vol. 3, No. 2, 1997, pp. 432–435.
   Book: 2. Kececioglu, D. B. and F.-B. Sun. 2002. *Burn-In Testing: Its Quantification and Optimization,* Lancaster, PA: DEStech Publications, Inc.

6. Tables. Number consecutively and insert closest to where first mentioned in text or type on a numbered, separate page. Please use Arabic numerals and supply a heading. Column headings should be explanatory and carry units. (See example at right.)

Table 5. Comparison of state-of-the-art matrix resins with VPSP/BMI copolymers.

Resin System	Core Temp. (DSC peak)	Char Yield, %
Epoxy (MY720)	235	30
C379: H795 = 14	285	53

7. Units & Abbreviations. SI units should be used. English units or other equivalents should appear in parentheses if necessary.
8. Symbols. A list of symbols used and their meanings should be included.
9. Page proofs. Authors will receive page proofs by E-mail. Proof pages will be in a .PDF file, which can be read by Acrobat Reader. Corrections on proof pages should be limited to the correction of errors. Authors should print out pages that require corrections and mark the corrections on the printed pages. Pages with corrections should be returned by FAX (717-509-6100) or mail to the publisher (DEStech Publications, Inc., 439 North Duke Street, Lancaster, PA 17602, USA). If authors cannot handle proofs in a .PDF file format, please notify the editors, Changfeng Ge at cfgmet@rit.edu or Bruce Welt at bwelt@ufl.edu.
10. Index terms.With proof pages authors will receive a form for listing key words that will appear in the index. Please fill out this form with index terms and return it.
11. Copyright Information. All original journal articles are copyrighted in the name of DEStech Publications, Inc. All original articles accepted for publication must be accompanied by a signed copyright transfer agreement available from the journal editor. Previously copyrighted material used in an article can be published with the *written* permission of the copyright holder (see #14 below).
12. Headings. Your article should be structured with unnumbered headings. Normally two headings are used as follows:

    Main Subhead: DESIGN OF A MICROWAVE INSTALLATION
    Secondary Subhead: Principle of the Design Method

13. If further subordination is required, please limit to no more than one (*Third Subhead*).
14. Equations. Number equations with Arabic numbers enclosed in parentheses at the right-hand margin. Type superscripts and subscripts clearly above or below the baseline, or mark them with a caret. Be sure that all symbols, letters, and numbers are distinguishable (e.g., "oh" or zero, one or lowercase "el," "vee" or Greek nu).
15. Permissions. The author of a paper is responsible for obtaining releases for the use of copyrighted figures, tables, or excerpts longer than 200 words used in his/her paper. Copyright releases are permissions to reprint previously copyrighted material. Releases must be obtained from the copyright holder, which is usually a publisher. Forms for copyright release will be sent by the editor to authors on request.

General: The *Journal of Applied Packaging Research* and DEStech Publications, Inc. are not responsible for the views expressed by individual contributors in articles published in the journal.